

DETAILED RESPONSE TO THE REVIEWER'S COMMENTS

We would like to thank the editor and the reviewer for re-reviewing the paper and providing the final comments. This manuscript has been improved significantly during the review process.

We have made a number of changes in response to the latest rounds of comments:

1. In response to the request for more discussion about how the models might be improved, two passages on how to improve the models have been added to the paper

Lines 416-424 now read

In BLING and miniBLING, by contrast, the biomass responds almost instantaneously to changes in growth conditions. This means that if the growth rate increases from 0.05 day^{-1} to 0.1 day^{-1} over the course of a month, the biomass associated with large phytoplankton will increase eightfold, even though the additional growth should only be enough to give an increase of a factor of $30 \text{ days} \times 0.05 \text{ day}^{-1} = 1.5$. Possibilities for addressing this effect include replacing the DOP tracer with a biomass tracer, which could then be partitioned between the different phytoplankton boxes based on the temporally smoothed growth rate, or increasing the timescale over which the growth rate is smoothed when biomass is calculated.

At lines 429-430 we state that the details of light limitation representation will be addressed in future research.

Lines 638-643

Overflows are difficult to simulate in level-coordinate models because they are prone to excessive entrainment of the dense plume (Winton et al., 1998). While significant effort has gone into simulating the Denmark Straits overflow at coarse resolution (Legg et al., 2009), our results show that smaller overflows such as the Persian Gulf may be regionally significant. This may provide further impetus for using isopycnal models in high resolution simulations, as such models can potentially simulate such overflows with greater fidelity.

2. All required technical corrections have been made.

3. The manuscript has been re-reviewed thoroughly by the authors and minor changes and spelling corrections have been made. For more clarity on the corrections, a corrected version of the manuscript that shows the corrections is accompanying this letter.

4. The quality of almost all figures has been enhanced via using a post-script format.

Sincerely

Safoura Seddigh Marvasti and Anand Gnanadesikan

Response to reviewer 2

I would like to express our appreciation to the Referee #2 for the comments.

Below, I respond to the comments, providing more elaboration or changing the manuscript if applicable.

1) The explanation given in the manuscript that "this is probably associated with the models mixing to excessive depth during the wintertime" (page 14, line 408/409) is very dissatisfactory. It may not be feasible to include a deeper analysis in this manuscript, but the authors could at least provide a discussion how the origin of the asymmetry in the observed nutrient dynamics may be investigated in further studies.

Response : The origins and also possibilities to address the issue are added to the manuscript as follows,

On page 14:

....

The equilibrium assumption, which means that biomass in both BLING and miniBLING is not directly simulated. In TOPAZ, the growth of plankton during the spring is limited by the biomass of phytoplankton, whereas in the fall TOPAZ continues to have higher heterotrophic biomass (diagnosed from growth rates over previous months) that then grazes the plankton. In BLING and miniBLING, by contrast, the biomass responds almost instantaneously to changes in growth conditions. This means that if the growth rate increases from 0.05 day^{-1} to 0.1 day^{-1} over the course of a month, the biomass associated with large phytoplankton will increase eightfold, even though the additional growth should only be enough to give an increase of a factor of $30 \text{ days} \times 0.05 \text{ day}^{-1} = 1.5$. Possibilities for addressing this effect include replacing the DOP tracer with a biomass tracer, which could then be partitioned between the different phytoplankton boxes based on the temporally smoothed growth rate, or increasing the timescale over which the growth rate is smoothed when biomass is calculated.

And also on page 21

Accordingly, there is a potential to improve the numerical models by better simulating the Persian Gulf Outflow to produce a sharper thermocline, allowing more realistic nutrient supply. Overflows are difficult to simulate in level-coordinate models because they are prone to excessive entrainment of the dense plume (Winton et al., 1998). While significant effort has gone into simulating the Denmark Straits overflow at coarse resolution (Legg et al., 2009), our results show that smaller overflows such as the Persian Gulf may be regionally significant. This may provide further impetus for using isopycnal models in high resolution simulations, as such models can potentially simulate such overflows with greater fidelity.

2) Technical corrections:

p. 4, l. 114: Resplandy et al. (2011) indicted that the spatial -> Resplandy et al. (2011) indicated that the spatial → Done (please see the manuscript).

p. 4, l. 122: with the specification four -> with the specification of four → Done (please see the manuscript).

p. 10, l. 286: macronutrient tracer Behrenfeld (2010). -> macronutrient tracer (Behrenfeld, 2010). → Done (please see the manuscript).

p. 10, l. 307: Within the smalle region the values are -> Within the small region, the values are → Done (please see the manuscript).

p. 18, l. 530: much water from Persian Gulf -> much water from the Persian Gulf → Done (please see the manuscript).

p. 20, l. 590: blooms in during certain times -> blooms during certain times → Done (please see the manuscript).

p. 20, l. 617/618: However, for a few cases eddies with a bloom -> However, for a few cases, eddies with a bloom → Done (please see the manuscript).

p. 20, l. 618/619: In this region consistency is observed -> In this region, consistency is observed → Done (please see the manuscript).

1 **Challenges in modelling spatiotemporally varying phytoplankton blooms in the**
2 **Northwestern Arabian Sea and Gulf of Oman**

3
4 **S. Sedigh Marvasti¹, A. Gnanadesikan², A.A. Bidokhti³, J.P. Dunne⁴, S. Ghader⁵**

5 [1] Department of Marine Sciences, Science and Research Branch, Islamic Azad University,
6 Tehran, Iran. (safoura.seddigh@gmail.com)

7 [2] Department of Earth and Planetary Sciences, Johns Hopkins University, Olin Hall, 3400
8 N. Charles St., Baltimore, MD 21218, USA. (gnanades@jhu.edu)

9 [3] Institute of Geophysics, University of Tehran, Tehran, P. O. Box 14155-6466, Iran.
10 (bidokhti@ut.ac.ir)

11 [4] National Oceanic and Atmospheric Administration/Geophysical Fluid Dynamics
12 Laboratory, 201 Forrester Rd., Princeton, NJ 08540-6649. (john.dunne@noaa.gov)

13 [5] Institute of Geophysics, University of Tehran, Tehran, P. O. Box 14155-6466, Iran.
14 (sghader@ut.ac.ir)

15 Correspondence to: S. Sedigh Marvasti (safoura.seddigh@gmail.com)

16

17 **Abstract**

18 Recent years have shown an increase in harmful algal blooms in the Northwest Arabian Sea
19 and Gulf of Oman, raising the question of whether climate change will accelerate this trend.
20 This has led us to examine whether the Earth System Models used to simulate phytoplankton
21 productivity accurately capture bloom dynamics in this region- both in terms of the annual
22 cycle and interannual variability. Satellite data (SeaWiFS ocean color) shows two
23 climatological blooms in this region, a wintertime bloom peaking in February and a
24 summertime bloom peaking in September. On a regional scale, interannual variability of the
25 wintertime bloom is dominated by cyclonic eddies which vary in location from one year to
26 another. Two coarse (1°) models with the relatively complex biogeochemistry (TOPAZ)
27 capture the annual cycle but neither eddies nor the interannual variability. An eddy-resolving
28 model (GFDL CM2.6) with a simpler biogeochemistry (miniBLING) displays larger
29 interannual variability, but overestimates the wintertime bloom and captures eddy-bloom

30 coupling in the south but not in the north. The models fail to capture both the magnitude of
31 the wintertime bloom and its modulation by eddies in part because of their failure to capture
32 the observed sharp thermocline/nutricline in this region. When CM2.6 is able to capture such
33 features in the Southern part of the basin, eddies modulate diffusive nutrient supply to the
34 surface (a mechanism not previously emphasized in the literature). For the model to simulate
35 the observed wintertime blooms within cyclones, it will be necessary to represent this
36 relatively unusual nutrient structure as well as the cyclonic eddies. This is a challenge in the
37 Northern Arabian Sea as it requires capturing the details of the outflow from the Persian Gulf-
38 something that is poorly done in global models.

39

40 1 Introduction

41 The region of northwestern Arabian Sea and the Gulf of Oman (15°–26° N, 56°–66°E)
42 is a highly productive region (Madhupratap et al., 1996; Tang et al., 2002), with satellite
43 estimates of carbon export of 137 gC/m²/yr, much higher than the ~80 gC/m²/yr found in the
44 Subpolar North Atlantic and Pacific (Dunne et al., 2007). Peak chlorophyll-a concentrations
45 exceed 0.7 mg/m³ in this region (Fig. 1a).

46 This region may be changing in important ways. In both the Persian Gulf and the Gulf
47 of Oman, there is evidence that harmful algal bloom (HABs) and their impacts are increasing
48 (Richlen et al., 2010). HAB occurrences have been more frequently reported in the Gulf of
49 Oman than in the Persian Gulf. A total of 66 red tide events (mostly dominated by *Noctiluca*
50 *scintillans*) have been recorded between 1976 and 2004 including 25 blooms resulting in mass
51 mortality of fish and marine organisms. Reasons for the increase in blooms include
52 aquaculture, industrial and sewage inputs, natural dispersal and human-aided transport, long-
53 term increases in nutrient loading and global expansion of species (Richlen et al., 2010) as
54 well as global climate change (Goes et al., 2005). The latter paper suggested that increasing
55 blooms were driven by an increase in the strength of the Asian monsoon.

56 Evaluating such a possibility and extending it into the future requires the use of Earth
57 System Models. However, such projections will only be as good as the models on which they
58 are based. In this paper we examine several models run at the Geophysical Fluid Dynamics
59 Laboratory in the Arabian Sea. We consider numerical results from five different 3D global
60 Earth system models, which we denote CORE-TOPAZ, Coupled-TOPAZ, Coupled-BLING,
61 Coupled-miniBLING, and the Geophysical Fluid Dynamics Laboratory Climate Model

Anand 1/7/2016 10:04 AM

Deleted: rather

Anand 1/7/2016 10:05 AM

Deleted: e activities

Anand 1/7/2016 10:05 AM

Deleted: and

Anand 1/7/2016 10:06 AM

Deleted: our

66 | version 2.6 (CM2.6 miniBLING). The first two of these models use the relatively complex
67 | TOPAZ biogeochemistry, but have low resolution and do not resolve eddies, the third has a
68 | simplified biogeochemistry (BLING, Galbraith et al., 2010) which does not carry
69 | phytoplankton biomass as a separate variable while the last two models have an even simpler
70 | biogeochemistry that does not directly simulate dissolved organic matter or iron cycling
71 | (miniBLING, Galbraith et al., 2015b). Only the final model resolves eddies.

72 | The seasonal cycle is an important metric for models to be able to simulate. The
73 | Arabian Sea is influenced by a reversing monsoonal cycle (Wang and Zhao, 2008), an
74 | evaporative fresh-water flux over most of the basin, and an annual mean heat gain (Banse and
75 | McClain, 1986; Fischer et al., 2002). In summer (June-September), the southwest Monsoon
76 | (SWM) blows strongly across the northwestern Arabian Sea (Al-Azri et al., 2010). Driven by
77 | a land-sea pressure gradient, the SWM is a large-scale feature of the atmospheric circulation
78 | of the tropics, extending from a surface pressure high near 30° S in the southern hemisphere
79 | northward to the surface low over Asia (Anderson and Prell, 1993). During the SWM, winds
80 | are steered by the East African highlands to form a strong low level atmospheric jet, referred
81 | to as the Findlater Jet (Bartolacci and Luther, 1999; Honjo et al., 2000), which crosses the
82 | Equator over the Indian Ocean and blows over the Arabian Sea parallel to the Omani
83 | coastline in a northeast direction (Honjo et al., 2000). The orientation of the Findlater Jet
84 | parallel to Omani coast leads to coastal upwelling along the coast and downwelling on the
85 | eastern side of the Jet in the middle of Arabian Sea. This upwelling provides nutrients to the
86 | surface layer (Fig. 1b) (Al-Azri et al., 2013; Kawamiya and Oschlies, 2003; Madhupratap et al.,
87 | 1996; Murtugudde et al., 2007; Veldhuis et al., 1997; Wang and Zhao, 2008). The SWM
88 | does not destabilize the surface layers, which are fairly stable in northern summer (Fig. 1c).

89 | The Northeast Monsoon (NEM), which happens from December through February, is
90 | not as strong as the SWM (Dickey et al., 1998; Shalapyonok et al., 2001; Veldhuis et al.,
91 | 1997). Ocean surface wind stress is lower (0.032 N/m² in NEM compared to 0.127 N/m² in
92 | SWM), and does not lead to upwelling like the SWM along the Omani coast. However,
93 | negative heat flux results in a destabilizing buoyancy flux, subsequent convective overturning
94 | (Barimalala et al., 2013; Kawamiya and Oschlies, 2003), and deepening and cooling to a
95 | depth of ~60m (Fig. 1c, 1d). This brings up nutrients and fuels a wintertime bloom. In
96 | addition, as shown in Fig. 1d in wintertime bloom the mixed layer depth (MLD) is deeper
97 | than summer.

Anand 1/7/2016 10:06 AM
Deleted:) (

Anand 1/7/2016 10:07 AM
Deleted: as very high resolution, but also a

Shahabeddin Tora..., 1/10/2016 10:44 AM
Deleted: (

Shahabeddin Tora..., 1/10/2016 10:45 AM
Deleted:)

Shahabeddin Tora..., 1/10/2016 10:44 AM
Deleted: Galbraith et al., 2015

Anand 1/7/2016 10:07 AM
Deleted: Biological cycling in CM2.6 is simulated using a modified version of the Biogeochemistry with Light Iron Nutrients and Gasses (BLING) model (Galbraith et al., 2010) called mini-BLING.

108 A second metric of the bloom dynamics is the relationship between the blooms and
109 mesoscale eddies (Al-Azri et al., 2013; Dickey et al., 1998; Hamzehei and Bidokhti, 2013;
110 Shalapyonok et al., 2001; Gomes et al., 2005). The confluence of the Persian Gulf outflow
111 current and the East Arabian Sea Current parallel to Omani and Yemeni coastlines in Arabian
112 Sea leads to formation of a frontal zone and formation of persistent eddies in the region.
113 Because the size of eddies is comparable to the width of the Gulf of Oman, they can affect
114 mixing and transport of biota on a basin scale (Fischer et al., 2002; Piontkovski et al., 2012).
115 Piontkovski et al. (2012) suggested that the increased amplitude of the seasonal cycle of
116 chlorophyll-a might be associated with the increased variability of mesoscale eddy kinetic
117 energy (EKE) per unit mass in the Gulf of Oman or in the western Arabian Sea. Gomes et al.
118 (2008) noted potential anticorrelation between sea surface height and chlorophyll, but did not
119 find a consistent relationship over time.

120 Gaube et al. (2014) provide a global overview of how eddies influence chlorophyll
121 blooms. They find that the effect of mesoscale eddies on the chlorophyll bloom varies both
122 temporally and spatially. They identify four particular mechanisms that can be distinguished
123 by linking sea surface anomalies to chlorophyll, namely eddy stirring, trapping, eddy
124 intensification, and Ekman pumping. Although Gaube et al. (2014) find a negative correlation
125 between chlorophyll and SSH in the Arabian Sea, they do not analyse which of these
126 mechanisms is involved in this region, nor do they quantify the extent to which this
127 correlation varies over the course of the season.

128 Resplandy et al. (2011) indicated that the spatial variability associated with mesoscale
129 eddies in the Arabian Sea produces spatial variability in the bloom and that another source of
130 variability is found to be restratification at these structures. Advection from coastal region is
131 identified as the mechanism providing nutrients in summer, while vertical velocities
132 associated with mesoscale structure are found to increase the overall nutrient supply.
133 However, this work does not make clear how the spatial distribution of the eddy nutrient
134 supply is related to the eddies, not whether this relationship is the same in all seasons.

135 The structure of this paper is as follows: all datasets including ocean color data and
136 altimeter data are explained in section 2 of the paper along with the specification of five
137 different 3D global Earth system models. In section 3, the remote sensing results are used to
138 study the spatiotemporal variability of chlorophyll-a in mesoscale structures in the study
139 region. We find a seasonal relationship between SSHA and chlorophyll such that cyclonic

Anand 1/7/2016 10:12 AM

Deleted: our

141 eddies are associated with blooms, but only during the winter. This means that interannual
 142 variability in blooms will be shaped by mesoscale eddy activity and may not be predictable.
 143 Results of the 3D global Earth system models are discussed in section 4. Annual cycles of
 144 variation of chlorophyll-a and nutrients for all GFDL models within the whole region are
 145 compared against the corresponding satellite results and field measurements. The models tend
 146 to overestimate wintertime productivity, in large part due to excessive mixing. They also fail
 147 to explain the bloom-SSHA relationship except in a few special cases. We argue that the
 148 eddies act to modulate turbulent mixing of nutrients to the surface- a mechanism not
 149 emphasized in previous literature. However, this can only occur if there is a strong and
 150 relatively shallow nutricline. Since the model only simulates such a feature in the Southern
 151 Arabian Sea, it does not capture the observed relationship between SSH and biology. Both the
 152 overestimation of the wintertime bloom and the failure to predict its modulation by eddies can
 153 thus be traced to difficulties in modeling the stratification of the Northwest Arabian Sea, most
 154 likely as a result of a failure to properly simulate overflows.

155

156 **2 Description of data and models**

157 **2.1 Satellite products**

158 We examine the relationship of blooms and eddies using the GSM5 Maritorena et al. (2002)
 159 product based on the SeaWiFS (Sea-viewing Wide Field-of-view Sensor) ocean color data
 160 and Sea Surface Height Anomaly (SSHA), based on altimeter data acquired from the
 161 Archiving, Validation and Interpretation of Satellite Oceanographic (AVISO) Data Center
 162 (<http://www.aviso.oceanobs.com>). The SSH anomaly is calculated relative to the annual
 163 cycle.

164 The GSM algorithm represents the normalized water leaving radiance $L_{wN}(\lambda)$ at multiple
 165 wavelengths as a nonlinear function, as following (Maritorena et al., 2002),

$$166 \hat{L}_{wN}(\lambda) = \frac{tF_0(\lambda)}{n_w^2} \sum_{i=1}^2 g_i \left\{ \frac{b_{bw}(\lambda) + b_{bp}(\lambda_0)(\lambda/\lambda_0)^{-\eta}}{b_{bw}(\lambda) + b_{bp}(\lambda_0)(\lambda/\lambda_0)^{-\eta} + a_w(\lambda) + Chl a_{ph}^*(\lambda) + a_{cdm}(\lambda_0) \exp[-S(\lambda - \lambda_0)]} \right\}^i \quad (1)$$

167 where t is the sea-air transmission factor, $F_0(\lambda)$ is the extraterrestrial solar irradiance, n_w is the
 168 index of refraction of the water, seawater backscatter $b_{bw}(\lambda)$, absorption $a_w(\lambda)$, a_{ph}^* is the
 169 chlorophyll-a (*chl*) specific absorption coefficient, S is the spectral decay constant for

170 absorption by chromophoric dissolved organic materials (CDOM), η is the power-law
171 exponent for the particulate backscattering coefficient, and λ_0 is a scaling wavelength (443
172 nm). The cdm absorption coefficient [$a_{cdm}(\lambda_0)$], and slope factor S then determine the
173 absorption across a range of wavelengths while the particulate backscatter coefficient [$b_{bp}(\lambda_0)$]
174 and coefficient η constrain the scattering. Letting λ_0 be 443 nm assuming that all terms other
175 than chl , [$a_{cdm}(\lambda_0)$] and $b_{bp}(443\text{nm})$ are constant, one can then use the [normalized](#) water
176 leaving radiance to invert for chl , a_{cdm} , and backscatter b_{bp} . One limitation of this approach is
177 that if the inherent optical properties vary with time [or space](#), this variation will introduce
178 errors into the estimate. Following Behrenfeld et al. (2005), we convert the backscatter
179 coefficient into units of particulate carbon biomass using the relationship $p_{carb}=13000(b_{bp}-$
180 $0.00035)$.

181 Satellite-based remote sensing is the only observational method suitable for measuring
182 physical and biological properties over large regions of the ocean. However, satellite ocean
183 color and SST are limited to surface distributions and provide no information about the
184 vertical structure within the ocean (McGillicuddy et al., 2001). Additionally acquiring data
185 requires cloud-free viewing of the ocean surface, which as we will see is a problem in this
186 region at certain times of the year. This lack of information motivates our examination of
187 numerical models, which ideally could be used to provide estimates of the ocean state when
188 observations are sparse as well as to extrapolate both vertically and into the future.

189

190 2.2 Numerical models

191 Numerical results are presented in this paper based on the output of [five](#) different 3D
192 global Earth system models, which we denote CORE-TOPAZ, Coupled-TOPAZ, Coupled-
193 BLING/miniBLING and GFDL CM2.6 (miniBLING). The first two of these models use the
194 relatively complex TOPAZ biogeochemistry, but have low resolution and do not resolve
195 eddies. The third [and fourth](#) use [two simplified biogeochemistry codes](#) (BLING and
196 miniBLING) which do not carry phytoplankton biomass as a separate variable while the last
197 model has very high resolution and uses the miniBLING simplified biogeochemistry. Below,
198 we describe the different physical models, followed by a summary of the biogeochemical
199 codes run within these models.

200

Anand 1/7/2016 10:22 AM

Deleted: our

Anand 1/7/2016 10:23 AM

Deleted: s

203 2.2.1 Physical model description

204 The ocean-ice model used in the CORE-TOPAZ model follows the corresponding
205 components of the GFDL CM2.1 global coupled climate model (Delworth et al., 2006). The
206 vertical resolution ranges from 10 m over the top 200 m to a maximum thickness of 250 m at
207 5500 m depth with 50 layers in all. The meridional resolution is 1°, whereas the zonal
208 resolution varies between 1° in mid-latitudes and 1/3° at the equator. North of 65°, a tripolar
209 grid is employed to avoid singularity arising from convergence of meridians at the North
210 Pole. Up-to-date parameterizations of mixed-layer dynamics, isopycnal mixing, advection by
211 subgridscale eddies, bottom topography, bottom flows, and lateral viscosity are included- for
212 more detail see Griffies et al. (2005) and Gnanadesikan et al. (2006). Both the dynamics and
213 thermodynamics sea ice are simulated with of five thickness classes of sea ice being resolved.

214 In the CORE-TOPAZ model, surface forcing is set using the Coordinated Ocean-ice
215 Reference Experiment (CORE) protocol (Griffies et al., 2009), where the inputs for
216 calculating surface fluxes are taken from an atmospheric analysis dataset adjusted to agree
217 better with in situ measurements. Sensible and latent heat fluxes are then calculated using
218 bulk formulae. Freshwater forcing is given by a combination of applied precipitation,
219 evaporation computed using bulk fluxes, and a correction diagnosed to restore surface
220 salinities in the top 10 m to climatological monthly values over 60 d. Hence, the fluxes
221 forcing the CORE runs could be thought of as “best guess” observationally based estimates.
222 Such a prescription omits important feedbacks whereby the atmosphere ensures that rainfall
223 and evaporation are consistent with each other, although the restoring correction is a crude
224 representation of these feedbacks. We use the version of the model described in Gnanadesikan
225 et al. (2011), which analyzed different modes of interannual variability in biological cycling
226 across the [North](#) Pacific Ocean.

227 The Coupled-TOPAZ model corresponds to the control simulation of the GFDL
228 ESM2M submitted as part of the IPCC AR5 process (Dunne et al., 2012). In this model the
229 ocean is coupled to the atmosphere, land, and sea ice components. Gnanadesikan et al. (2014)
230 discuss the behavior of this model in the North Atlantic, but its behavior in the Arabian Sea
231 has not been previously analyzed. Two additional versions of this model, referred to here as
232 Coupled-BLING/[miniBLING](#), [were](#), run using the BLING and mini-BLING biogeochemical
233 models described below, but with the light field given by the TOPAZ code. The differences
234 between the 1-degree models [highlight](#) differences due to biological formulation.

Anand 1/7/2016 10:25 AM

Deleted: as

Anand 1/7/2016 10:25 AM

Deleted: emphasizes

237 The ocean component of ESM2M employs the MOM4p1 code of Griffies et al. (2009)
238 which largely mimics the CM2.1 ocean (identical horizontal and vertical resolution and
239 parameterization of mixing). However, ESM2M ocean uses a rescaled geopotential vertical
240 coordinate (z^* ; Adcroft et al., 2004; Stacey et al., 1995) for a more robust treatment of free
241 surface undulations. The ESM2M implementation includes updates to the K-profile
242 parameterization (Large et al., 1994) based on Danabasoglu et al. (2006), as well as model-
243 predicted chlorophyll modulation of short-wave radiation penetration through the water
244 column. ESM2M also includes completely novel parameterizations relative to CM2.1, such as
245 parameterization of submesoscale eddy-induced mixed layer restratification (Fox-Kemper et
246 al., 2008). Instead of prescribed vertical diffusivity for interior mixing (Bryan and Lewis,
247 1979), ESM2M employs the Simmons et al. (2004) scheme along with a background
248 diffusivity of $1.0 \times 10^{-5} \text{ m}^2 \text{ s}^{-1}$ in the tropics and $1.5 \times 10^{-5} \text{ m}^2 \text{ s}^{-1}$ poleward of 30° latitude
249 following a *tanh* curve.

250 The Geophysical Fluid Dynamics Laboratory Climate Model version 2.6 (CM2.6) is a
251 high-resolution eddy-resolving model. This model has the same atmosphere model and ocean
252 Physics as CM2.5 (Delworth et al., 2012). CM2.6's ocean component has higher horizontal
253 resolution than CM2.5, with grid spacing, which is changeable from 11 km at the equator to
254 less than 4 km at very high latitudes. This means that the model is capable of resolving eddy
255 features in the tropics, as we will see below.

256

257 2.2.2 Biogeochemical Cycling codes

258 The TOPAZ code (Tracers of Ocean Productivity with Allometric Zooplankton code
259 of Dunne et al., 2010), keeps track of five inorganic nutrients used by phytoplankton: nitrate
260 and ammonia, inorganic phosphate, silicate, and dissolved iron. Additionally, the model
261 carries three other dissolved inorganic tracers: dissolved inorganic carbon, alkalinity and
262 dissolved oxygen. Based on the work of Dunne et al. (2007), the model also keeps track of
263 fine lithogenic material, which plays a role in ballasting organic material and delivering it to
264 the sediment (Armstrong et al., 2002; Klaas and Archer, 2002). The five inorganic nutrients
265 are taken up in different ways by three classes of phytoplankton: small, large and
266 diazotrophic. A comprehensive description of TOPAZ v2 can be found in the supplemental
267 material of Dunne et al. (2013).

Shahabeddin Tora..., 1/10/2016 11:02 AM

Formatted: Font:(Default) Times New Roman

Shahabeddin Tora..., 1/10/2016 11:02 AM

Formatted: Font:(Default) Times New Roman

Shahabeddin Tora..., 1/10/2016 11:02 AM

Formatted: Font:(Default) Times New Roman

268 TOPAZ is unusual among comprehensive Earth System Models in that it uses a highly
269 parameterized version of grazing. Instead of grazers being explicitly simulated, grazing rates
270 are simply taken as a function of phytoplankton biomass, with different power-law
271 dependence for small and large phytoplankton. The grazing formulation was fit to about 40
272 field sites to produce a size structure that transitions realistically between being dominated by
273 small phytoplankton and low particle export ratio at low levels of growth and large
274 phytoplankton and high particle export ratio in nutrient and light-replete conditions. At
275 equilibrium, the resulting parameterization produces biomass that is a function of growth rate
276 (linear for small plankton, cubic for large). A similar scaling in particle size spectrum was
277 seen across ecosystems by Kostadinov et al. (2009). In contrast to models that explicitly
278 simulate zooplankton, TOPAZ, does not depend on poorly known zooplankton behavioral
279 parameters (such as handling efficiency or grazing half-saturation) or on the details of how
280 different trophic levels interact.

281 Even though it does not simulate zooplankton explicitly, TOPAZ still carries over two
282 dozen tracers, making it extremely expensive to run in high-resolution simulations. For this
283 reason Galbraith et al. (2010) developed the Biogeochemistry with Light Iron Nutrients and
284 Gasses (BLING) model, which parameterizes the entire ecosystem. The original version of
285 BLING has only five explicit tracers: dissolved inorganic phosphorus (PO_4), dissolved
286 organic phosphorus (DOP), dissolved Iron (Fe), dissolved inorganic carbon (DIC), and
287 oxygen (O_2). It includes the impacts of macronutrient and micronutrient limitation and light
288 limitation on phytoplankton by using these to calculate a growth rate. Using the same
289 machinery as TOPAZ, it then uses this growth rate and implicit treatment of community
290 structure to estimate phytoplankton biomass, and uses this biomass to calculate the rate at
291 which nutrient is taken up by plankton and cycled through the ecosystem.

292 The miniBLING code (Galbraith et al., 2015) represents a further simplification. In
293 this model the iron field is taken from a lower-resolution version of the model (an
294 approximation which has limited impact in the Arabian Sea, where phytoplankton are
295 generally not iron-limited) and so Fe is not treated prognostically. Additionally the DOP pool
296 is eliminated. Simulations using the ESM2M physical model show that control simulations of
297 oxygen and surface nutrients produced by the miniBLING and BLING models are very
298 similar to those produced in the same model with TOPAZ (Galbraith et al., 2015). Galbraith
299 et al. (2015), also show that BLING and miniBLING simulate very similar patterns of oxygen

Anand 1/7/2016 10:27 AM

Deleted: it

Anand 1/7/2016 10:27 AM

Deleted: n to

Anand 1/7/2016 10:28 AM

Deleted: (Galbraith et al., 2010)

Shahabeddin Torab..., 1/10/2016 9:57 AM

Formatted: Subscript

Anand 1/7/2016 10:29 AM

Deleted: DIC (

Anand 1/7/2016 10:30 AM

Deleted: This manuscript

Anand 1/7/2016 10:30 AM

Deleted: s

306 change and anthropogenic uptake in a simulation where CO₂ is increased by 1% per year
307 until it [is twice the preindustrial concentration](#).

308 It should be noted that simplified BLING and miniBLING codes neglect some
309 processes that may be important. Only nonliving components are advected and mixed by the
310 ocean circulation, which could result in inaccurate distribution of biology in frontal regions at
311 high resolution. [Additionally, as will be discussed below, the lack of a biomass variable may](#)
312 [lead to overestimating how rapidly plankton inventories can grow](#). Also, the rich behavior of
313 the nitrogen cycle with its interaction with iron, phosphorus and oxygen cannot be simulated
314 with one macronutrient tracer (Behrenfeld 2010). Specifying iron limitation, as done in
315 miniBLING, may also have some impacts in our region. As extensively discussed by Naqvi et
316 al., (2010) there is a possibility of iron limitation over the southern parts of the Omani shelf
317 and in the offshore region during the latter part of the Southwest Monsoon, which can result
318 in high nitrate-low chlorophyll conditions. The western equatorial and southern tropical
319 region of the Indian Ocean are iron-limited and the Arabian Sea (southern parts) may become
320 iron-limited under strong upwelling conditions (Wiggert et al., 2006).

321

322 3 Remote sensing results

323 3.1 Annual cycle and interannual variability

324 We begin by using the GSM5 satellite data to examine the annual cycle and interannual
325 variability in two different regions, the whole NW Arabian Sea (56°-66° E, 15°-26° N) and a
326 smaller region including the Gulf of Oman, (60°-62° E, 22°-26° N). As shown in Fig. 2 (a) to
327 (c) for whole region, clear annual cycles of chlorophyll-a, backscattering and CDOM are
328 observed. Even larger annual cycles of variation of chlorophyll-a, backscattering and CDOM
329 are seen in the smaller region, as shown in Fig. 2 (d) to (f). More pronounced interannual
330 variability is observed in the smaller region as opposed to the larger region.

331 The annual variations of all parameters are broadly consistent with each other. The maximum
332 values associated with the summer bloom are generally seen in September, with values of 1.0
333 mg/m³, 50 mgC/m³, and 0.1 m⁻¹ for chlorophyll, particulate carbon and CDOM, respectively,
334 within the whole region. Within the smaller region, the values are 1.25 mg/m³, 65 mgC/m³,
335 and 0.125 m⁻¹ for chlorophyll, particulate carbon, and CDOM, respectively. For two years of
336 2001 and 2002, the particulate carbon values (~90 mgC/m³) are much higher than the average

Anand 1/7/2016 10:30 AM

Deleted: doubles

Shahabeddin Torabian 1/6/2016 8:59 PM

Deleted: (

Anand 1/7/2016 10:33 AM

Deleted: I

Anand 1/7/2016 10:34 AM

Deleted: e

341 of the other months over both regions, but the chlorophyll does not show pronounced peaks.
342 A winter bloom is also pronounced in February as a second maximum in a yearly cycle,
343 where the magnitudes are about 0.07 mg/m³, 40 mgC/m³, and 0.07 m⁻¹ for chlorophyll,
344 particulate carbon and CDOM, respectively, within the whole region, and about 0.09~1.5
345 mg/m³, 55~80 mgC/m³, and 0.11~0.14 m⁻¹ for chlorophyll, particulate carbon and CDOM,
346 respectively, within the smaller region. That the summer bloom in the both regions is stronger
347 than the winter bloom has been discussed by Al-Azri et al. (2010), and Levy et al. (2007).

Anand 1/7/2016 10:35 AM

Deleted: mgC/m³

Anand 1/7/2016 10:36 AM

Deleted: mgC/m³

348 3.2 Variability of Chlorophyll-a in Mesoscale Structures

349 Mesoscale structures can be seen in the Northwest Arabian Sea in both the SeaWiFS
350 chlorophyll-a distribution and AVISO sea surface height anomaly. Over the course of 2001
351 (Fig. 3), both a summer bloom (which most likely starts in August and ends in ~October) and
352 a winter bloom (which starts in January and goes away in April) can be seen in chlorophyll-a.
353 In March, the last month of the winter bloom, chlorophyll-a concentrations are high over the
354 entire region in both the anticyclones (warm eddies with positive SSHA) and the cyclones
355 (cold eddies with negative SSHA). The observed bloom in March terminates abruptly in
356 April, although the observations show that eddies are still active in the region. In June, July
357 and August, the satellite ocean color data is not available due to excessive cloudiness. In
358 September, the last month of the summer bloom, most of the region including cyclones and
359 anticyclones and coastal regions had high chlorophyll-a concentration. However in the
360 following months the bloom persists only within the cold eddies and disappears over the
361 warm eddies (a phenomenon also seen in Sargasso Sea by McGillicuddy et al., 2001). The
362 relationship between sea surface chlorophyll-a and eddies for the other years between 1998
363 and 2005 during the month of November, is shown in Fig. 4. The relationship between
364 blooms and SSHA is clear and striking. Note particularly the difference between 1998 and
365 2001, when the location of high and low chlorophyll regions switches relative to the Ras al
366 Hadd. This difference in bloom location is perfectly reflected in the different locations of the
367 eddies.

Anand 1/7/2016 10:37 AM

Deleted: patterns

368 3.3 Chlorophyll-Sea Surface Height Anomaly (SSHA) cross-correlation

369 The seasonal relationship between chlorophyll and SSHA can be seen in the monthly
370 variation of the spatial cross-correlation between the two variables over the entire northwest
371 Arabian Sea. chlorophyll-SSHA cross-correlations between 1998 and 2005 in the satellite

375 data are shown in Fig. 5a. To check that the chlorophyll results are not an artifact of the
376 remote sensing inversion, two other related parameters, the backscattering coefficient (BBP)
377 and chromophoric dissolved organic matter (CDOM) are also cross-correlated with SSHA, as
378 depicted in Figs. 5b and c. The results show consistent annual cycles of variation in the cross-
379 correlation of all three variables. This suggests a repeatable yearly phenomenon in the region
380 as discussed in the previous sections. The cross-correlation results over the 8 years of study
381 show that there are several months (i.e. November-December) with relatively high anti-
382 correlation for most of the years and also several other months (i.e. April-May) with no or
383 even low positive correlation.

384 The averaged climatological monthly cross-correlation with SSHA and climatological
385 monthly values between 1998 and 2005 are shown in Fig. 6 for all parameters. Two blooms
386 ending in March (winter) and September (summer) are seen. At the peak of the blooms the
387 average cross-correlation values are very low due to the existence of blooms in both cyclones
388 and anticyclones. The months after the winter and summer blooms show a clear difference in
389 the correlation. After the winter bloom (typically April and May), the cross-correlation is
390 positive or very small, which suggests no relation between the mesoscale eddies and the
391 blooms. As discussed in Kumar et al. (2001), low primary production is observed after
392 termination of winter cooling during Spring Inter-Monsoon (SIM) (see also Gomes et al.,
393 2008). This result would be also consistent with SIM producing weak atmospheric forcing in
394 the region.

395 In contrast, after the summer bloom (typically October-December) as the average values of
396 chlorophyll-a decrease, chlorophyll and SSHA become relatively highly anti-correlated. The
397 reason for the anti-correlation is the persistence of chlorophyll at the regions with negative
398 SSHA that are typically considered to be cyclonic (cold) eddies and disappearance of
399 chlorophyll-a in positive SSHA that are assumed to be anti-cyclonic (warm) eddies. Particle
400 backscatter also provides almost same cross-correlation, suggesting that the chlorophyll-a
401 signal does not result purely from photo-adaptation. Moreover, the CDOM-SSHA cross-
402 correlation shows the same annual cycle, although with smaller peak values.

403 The spatial relationship between blooms and eddies seen in the Northern Arabian Sea can be
404 compared with the patterns noted by Gaube et al. (2014). Their eddy stirring mechanism
405 involves advection of high and low chlorophyll signals around an eddy, resulting in a low
406 which is offset from the center of an anticyclone and a high which is offset from the center of

Anand 1/7/2016 10:38 AM

Deleted: s

Shahabeddin Torab..., 1/12/2016 8:17 PM

Deleted: ,

Anand 1/7/2016 10:40 AM

Deleted: and average value results

Anand 1/7/2016 10:41 AM

Deleted: patterns for bloom tim

Anand 1/7/2016 10:41 AM

Deleted: es but typically shows

Anand 1/7/2016 10:42 AM

Deleted: lower

Anand 1/7/2016 10:42 AM

Deleted: correlation

414 a cyclone. Ekman pumping would be expected to produce negative anomalies in cyclones
415 with a positive “halo” and positive anomalies in anticyclones with a negative “halo” (Gaube
416 et al. (2014), Fig. 2). Trapping of chlorophyll involves eddies retaining the properties that
417 they had when shed from a boundary current, which would generally imply low values in
418 anticyclones and high values in cyclones. Eddy intensification would be expected to produce
419 the same picture, as cyclones would see rising nutriclines in the center but anticyclones would
420 see deepening nutriclines. The basic picture seen in the Arabian Sea is inconsistent with the
421 first two mechanisms but is potentially consistent with the second two. However, without in-
422 situ data it is impossible to validate either of these mechanisms.

423

424 **4 Numerical modelling results**

425 **4.1 Temporal variability**

426 | [Time series](#) of chlorophyll-a, phosphate and nitrate for all GFDL models are shown in Fig. 7a
427 to c within the whole region and compared against the corresponding GSM5 satellite results
428 or WOA09. Note that the eight years of the model output, selected as the last eight years of
429 the run, would not be expected to correspond to the eight actual years in the satellite data. The
430 annual cycles of chlorophyll-a and biomass are quite similar to each other in all GFDL
431 models, insofar as they show two distinct blooms in yearly cycle. The maximum values that
432 can be considered as a winter bloom in the whole region are mostly seen around February
433 | (Piontkovski et al., 2011), with values of 0.32–0.38, 0.48–0.62, 1.0–2.0, 1.5–2.2, 0.8–1.6, [and](#)
434 0.6–0.75 mgm⁻³ for chlorophyll in CORE-TOPAZ, Coupled-TOPAZ, CM2.6 (miniBLING),
435 miniBLING (Low resolution), BLING and satellite data, respectively. A summer bloom is
436 also pronounced in September as a second maximum in the yearly cycle over the whole
437 | region, with peak magnitudes of about 0.25–0.52, 0.65–0.7, 0.65–1.15, 0.8–1.15, 0.5–0.75, [and](#)
438 0.75–1.3 mgm⁻³ for chlorophyll across the different datasets.

439 Notice the results from the BLING model run in the coarser resolution ESM2M code (purple
440 lines). The differences between BLING and miniBLING (light blue lines) in this code are just
441 | due to having fixed iron [and no dissolved phosphorus](#) in miniBLING. The light field in these
442 ESM2M runs is computed from using TOPAZ-derived chlorophyll, so that all three models
443 see identical physical conditions. Both BLING and miniBLING in ESM2M produce an
444 asymmetry in chlorophyll between February and September that is similar to that produced in

Anand 1/7/2016 10:43 AM

Deleted: Annual cycles of variation

446 CM2.6 miniBLING. This asymmetry is not seen in TOPAZ. Analysis of what drives this
447 asymmetry shows that it is not straightforward. All of the model runs show an asymmetry in
448 the nutrient concentrations that is in the opposite direction as the observations, with higher
449 nutrients in February than in September, as shown in Fig 7b. As we will show later in the
450 manuscript, this is probably associated with the models mixing to excessive depth during the
451 wintertime. However, in TOPAZ this does not produce an asymmetry in chlorophyll, while in
452 BLING and miniBLING it does. There are two possible reasons for this:

453 1) The equilibrium assumption, which means that biomass in both BLING and miniBLING is
454 not directly simulated. In TOPAZ, the growth of plankton during the spring is limited by the
455 biomass of phytoplankton, whereas in the fall TOPAZ continues to have higher heterotrophic
456 biomass (diagnosed from growth rates over previous months) that then grazes the plankton. In
457 BLING and miniBLING, by contrast, the biomass responds almost instantaneously to changes
458 in growth conditions. This means that if the growth rate increases from 0.05 day^{-1} to 0.1 day^{-1}
459 over the course of a month, the biomass associated with large phytoplankton will increase
460 eightfold, even though the additional growth should only be enough to give an increase of a
461 factor of $30 \text{ days} \times 0.05 \text{ day}^{-1} = 1.5$. Possibilities for addressing this effect include replacing the
462 DOP tracer with a biomass tracer, which could then be partitioned between the different
463 phytoplankton boxes based on the temporally smoothed growth rate, or increasing the
464 timescale over which the growth rate is smoothed when biomass is calculated.

465 2) Different handling of light limitation. In TOPAZ light limitation is calculated using the
466 instantaneous local light, whereas in BLING it is calculated using the mixed layer average
467 light. Preliminary results with a very coarse resolution model using BLING show that this
468 reduces the summer-winter asymmetry slightly, but is not sufficient to make the February
469 bloom smaller than the September bloom. This effect will also be addressed in future
470 research.

471 It is likely that all three of these factors- too deep winter mixed layers leading to too high
472 nutrients, too little light limitation and instantaneous response to changes in growth
473 conditions, are all responsible for the overly strong blooms in boreal winter in the Arabian
474 Sea.

475 To get a better sense of the mechanisms driving the blooms in the model, the biomass (mol P
476 kg^{-1}) of the miniBLING CM2.6 model is compared with the light intensity in the mixed layer
477 and the light-saturated photosynthesis rate (carbon specific) (s^{-1}) in Figs. 8a and b for January

Anand 1/7/2016 10:48 AM

Formatted: Superscript

Anand 1/7/2016 10:48 AM

Formatted: Superscript

478 of year 195. The two terms in Fig. 8 are the two terms in the model that affect growth rate.
479 Because biomass in the miniBLING model is a function of growth rate only, [understanding](#)
480 [the variation in two terms is sufficient to understand what drives the variation of biomass](#) in
481 the model. The biomass production and mixed layer light intensity (Fig. 8a) are not
482 meaningfully correlated parameters. On the other hand, the biomass and the light-saturated
483 carbon specific growth rate (Fig. 8b; indicating the degree of nutrient limitation) are
484 positively correlated. From this, it can be concluded that the blooms in this region are more
485 driven by nutrient rather than light, consistent with, for example, Gomes et al. (2008). This
486 suggests in turn that it is likely biases in nutrient supply that drive biases in productivity.

487 We can get more insight into nutrient biases by examining the individual tendency terms
488 associated with advection, vertical diffusion and subgridscale eddy fluxes and time rate of
489 change of nutrients. For simplicity, in this paper we combine the vertical diffusive flux
490 associated with small-scale mixing [from the background diffusion](#) with that due to the mixed
491 layer parameterization. Fig. 9 shows PO₄ advection, diffusion and [time](#) tendency flux terms
492 for the whole region (56°-66°E, 15°-26°N) over a typical year. [We calculate these by,](#)
493 [integrating the time tendency terms for phosphate over the top 50m.](#) The results show that the
494 dominant source in whole region during the winter bloom is diffusion, suggesting the model
495 predicts excessively strong mixing during the wintertime. By contrast, the advection
496 dominates diffusion [during the summer bloom,](#) supplying the [majority of](#) nutrients, during the
497 months of July and August. [The fact that the summertime bloom is close to observations](#)
498 suggests that the model correctly simulates this wind-driven upwelling.

499 In addition to having annual cycles that are different from observations, the models also differ
500 from data in terms of interannual variability. As shown in Fig. 10, low-resolution models
501 (CORE- and coupled-TOPAZ) provide an almost uniform seasonal coefficient of variation
502 (mean C.o.Vs are 0.15 and 0.18, respectively), while both data and eddy resolving CM2.6
503 models show higher interannual variability and seasonal changes (mean C.o.Vs are 0.35 and
504 0.5, respectively). The C.o.Vs are particularly higher during the winter and summer blooms in
505 the observations, while the low-resolution models do not see these signals. In other words, the
506 low-resolution models fail to get enough variability, while the high-resolution models produce
507 too much interannual variability. Together with the Fig. 4, this statistical analysis suggests
508 that eddies are necessary to explain the variability in the data as opposed to the low-resolution

Anand 1/7/2016 10:55 AM

Deleted: it is in fact sufficient to understand what drives the growth

Shahabeddin Tora..., 1/10/2016 10:04 AM

Deleted: 10

Anand 1/7/2016 10:58 AM

Deleted: , which is

Anand 1/7/2016 10:58 AM

Deleted: averaged flux values over the upper 50 meter calculated for phosphate (PO₄).

Anand 1/7/2016 10:59 AM

Deleted: in

Anand 1/7/2016 10:59 AM

Deleted: particularly

Anand 1/7/2016 10:59 AM

Deleted: and

Anand 1/7/2016 10:59 AM

Deleted: t

519 | models, [but that the high-resolution model does not properly capture this variability](#). Below,
520 | we examine the relationship of eddies and blooms in the high-resolution models.

521

522 | **4.2 Blooms and sea surface height in CM2.6**

523 | **4.2.1 Large-scale correlation**

524 | The relationship between SSHA and chlorophyll is quite different in the model as compared
525 | to the satellite. Monthly variation in the cross-correlation of chlorophyll and SSHA for eight
526 | consequent years in CM2.6 is shown in Fig. 11. As in the remote sensing, the model shows
527 | annual cycles of variation in the cross-correlation, suggesting a repeatable yearly phenomenon
528 | in the region. However the structure of this annual cycle is not consistent with the satellite
529 | data. The model predicts several months (i.e. March-August) with anti-correlation for most of
530 | the years, but with values less than 0.5, smaller than the peak anti-correlation values in
531 | satellite results. The model also predicts that several other months (i.e. October-February)
532 | should have no or even positive correlation, while the satellite shows strong negative
533 | correlations during these months.

534

535 | **4.2.2 Blooms in Mesoscale Structures**

536 | Why does the GFDL CM2.6 model not produce the same relationship between SSHA and
537 | chlorophyll as the satellite? We can gain some insight by examining snapshots of the two
538 | fields. In Figs. 12a and b, sea surface chlorophyll-a concentration and sea surface height
539 | anomaly (SSHA) are shown at two snapshots of time, November 9th and December 28th for
540 | model year 195. Comparing the figures with the corresponding satellite results in Fig. 3 for
541 | the months of November and December, we see that the southern part of the GFDL model is
542 | more similar to the satellite data, with high concentrations of chlorophyll-a tending to be
543 | located at the center of cyclones. In contrast, in the northern part of the region, the GFDL
544 | model predicts high chlorophyll at the edges of the cyclones as well as in the center of
545 | anticyclones. The eddy structures have smaller diameters in GFDL results than the field
546 | observations, though it is not clear whether this represents smoothing in the AVISO product
547 | or some physical weakness of the model.

548 We now focus on the few examples in our model output where chlorophyll blooms are found
549 in the center of cyclonic eddies. These are denoted as E1 and E2 in Figs. 12a and b. To track
550 the movement of the selected eddies, E1 and E2, over the time from November 9th to
551 December 28th, modeled chlorophyll and SSHA are shown in Figs. 12c and d along two
552 different latitudes, 16°N (for E1) and 19°N (for E2). Fig. 12c shows that E1 moved westward
553 during this period of time, and that the chlorophyll concentration was kept high within the
554 central part of the eddy. E1 appears to be created by the passage of a cyclone, similar to the
555 eddy observed by Wang and Zhao (2008) in the aftermath of Cyclone Gonu. Similarly, as
556 shown in Figs. 12d, E2 was a persistent eddy with both central and edge blooms during the
557 month of November that started to move towards the west during the December along 19°N.
558 However, at other latitudes, the largest blooms offshore are found along gradients in SSH
559 rather than being associated with maxima or minima. This suggests a different mechanism for
560 producing blooms in the model. Following Gaube et al. (2014), it appears that the eddy
561 stirring mechanism is dominant. Satellite data (i.e. see Fig. 3 for the month of May) provide
562 some hints of high-chlorophyll plumes being advected away from coastal regions. As shown
563 in Figs. 12a and b, high velocities in the marginal region between adjacent cyclonic and
564 anticyclonic eddies can cause such plumes in the GFDL models as well.

565 Why is the model only able to simulate the relationship between SSH and chlorophyll in the
566 southern part of the domain? We hypothesize this is due to differences in stratification
567 between the two regions. The average water temperature (colors) and the macronutrient (PO₄)
568 concentrations (contours) for model year 197 are compared to the corresponding measured
569 values in World Ocean Atlas (WOA09) within the upper 200m in the northern (60°-66°E and
570 19°-23°N) and southern (60°-66°E and 15°-17°N) part of the region are shown in Fig. 13. In
571 the northern part of the region (see Fig 13a and b), the GFDL model provides a reasonably
572 good estimation of the mean temperature field near the surface, but subsurface temperatures
573 are not as consistent as there is far too little stratification. This is also associated with a very
574 weak nutricline in CM2.6. Variations in isopycnal depth will therefore not lead to big
575 differences in nutrient supply. Figs. 13c and d show the same fields for the southern part of
576 the region. Unlike the northern part of the domain, the temperature gradient over these depths
577 is well estimated by CM2.6. While the nutricline is still too weak there is some gradient in
578 nutrients between 80 and 120m.

579 As seen in Fig. 1d, both the ARGO and WOA09 wintertime mixed layer depth is considerably

Anand 1/7/2016 11:03 AM
Deleted: for the existence
Anand 1/7/2016 11:03 AM
Deleted: advective

Anand 1/7/2016 11:03 AM
Deleted: s
Shahabeddin Torab..., 1/10/2016 9:57 AM
Formatted: Subscript

Shahabeddin Torab..., 1/12/2016 8:22 PM
Deleted: results

Anand 1/7/2016 11:04 AM
Deleted: (
Anand 1/7/2016 11:04 AM
Deleted:)

586 deeper than the [summertime mixed layer depth](#), reaching a maximum of 65m. However, in
587 the northern regions [of the model](#) the MLD seems to be too deep in winter, reaching values of
588 130-150 m. This suggests that the overly deep mixed layer in the northern part of the region
589 may explain both the tendency towards an overly strong winter bloom and the failure of
590 mesoscale eddies in modulating chlorophyll blooms. If we look during the time period where
591 we have eddies E1 and E2 (Nov-Dec. year 197, Fig 6c,d) we see shallower mixed layers
592 associated with both eddies.

593 Both the temperature and mixed layer biases in the northern part of the Arabian Sea may
594 result from having too much water from [the Persian Gulf](#) in this region. This can be seen in
595 the yearly averaged subsurface salinity-density distribution over the region, shown in Figs 13e
596 and f for both WOA09 data and CM2.6 (model year 197), respectively. Fig. 13e shows two
597 separate tongues of salty water, one near the surface and one at the depth of ~300m. These
598 salty water signals are consistent with the seasonal cycle of Persian Gulf outflow as discussed
599 in Ezam et al. (2010). On the other hand, CM2.6 shows one subsurface salty water signal
600 from the northern part, which is deep and strong enough to result in weak stratification in the
601 north to a depth of 250m, as shown in Fig. 13f. These results suggest that a sharp thermocline
602 and nutricline is necessary for eddy activity to modulate the mixing of nutrients to the surface.

603 We test the idea that a sharper thermocline could modulate mixing of nutrients to the surface
604 by looking at the sources of nutrient in the southern part of Arabian Sea where eddy-bloom
605 relationships [similar to observations](#) are [occasionally](#) seen. Accordingly, the region containing
606 eddy E1 in Fig. 12 is analyzed to determine the physical mechanisms by which nutrient is
607 transported into the surface layer. Fig. 14 contrasts chlorophyll concentration, advection, and
608 diffusion terms for the region from 63°-66°E, 15°-18°N over the December of two consecutive
609 CM2.6 years of 197 and 198. In [December of year 197](#) we see an eddy associated with a
610 bloom while there is no eddy in [December of year 198](#), and the chlorophyll concentrations are
611 much lower. In both years the diffusive flux of nutrient to the top 50m mirrors the
612 chlorophyll. But in 197 it is larger and positive (~10 mol/m²/month) in the eddy while the
613 advective flux is actually negative in this region. By contrast in Year 198, there is no cyclonic
614 eddy and the diffusive fluxes are much smaller.

615 The bloom associated with eddies E1 and E2 do not fit with any of the mechanisms
616 highlighted in Gaube et al. (2014). We first consider the mechanism of trapping. Eddy E1 is
617 generated in the ocean interior, not as a result of coastal upwelling. As shown in Fig. 15, the

Anand 1/7/2016 11:04 AM

Deleted: at of

Shahabeddin Torab..., 1/10/2016 1:18 PM

Deleted:

Anand 1/7/2016 11:07 AM

Deleted: Y

Anand 1/7/2016 11:07 AM

Deleted: at the same time

622 nutrient supply rate ranges between 5 and 8 mmol/m²/month in the eddy. The concentrations
623 in this eddy are only 0.01 μM (5 mmol/m²) over the top 50 m. It cannot be the case that the
624 nutrients in the eddy can last for several months as a result of “trapping”, there must be a
625 continuous supply. Moreover although eddy E2 shows a horizontal advection signal in
626 November (with a positive ring around the edge in Fig. 12a), the signal in December has the
627 opposite sign. Eddy intensification is also an unlikely mechanism for explaining the blooms,
628 as $dSSH/dt$ is relatively small (particularly if we track the minimum SSH associated with E1
629 in Fig. 12c or E2 in Fig. 12d). Finally, Ekman pumping signatures in Gaube et al. (2014) have
630 the opposite sign as what is seen in E1 and E2.

631 Our results also contrast with those in Resplandy et al. (2011). The focus in Resplandy et al.
632 (2011) is on the productivity driven by horizontal and vertical advection in summer and
633 mostly vertical advection in winter. This contradicts our finding of a primary diffusive source
634 of nutrient in winter although it is consistent the finding of advective source of nutrients in
635 summer. We point out that in our model, the only two eddies that actually look like what we
636 see in the satellite observations involve enhanced mixing from below. This is a different result
637 from Levy et al. (2014) and Resplandy et al. (2011). Moreover it is not clear whether these
638 papers get the seasonal correlation with SSH or not. Resplandy et al. (2011) do not focus on
639 structures at the eddy scale as they are more concerned with the net impact of eddies.

640

641 To summarize, we hypothesize that

642 1. The reason that blooms are found in cyclones in the Arabian Sea during the NEM is that
643 the dominant source of nutrients to the surface, i.e. mixing (Barimalala et al., 2013;
644 Kawamiya and Oschlies, 2003) is concentrated there.

645 2. Interannual variability in wintertime blooms in the Northwest Arabian Sea is controlled by
646 the combined presence of these eddies and strength of wintertime cooling.

647 3. Excessive mixing (resulting in too weak a thermocline) prevents mixing from being
648 modulated by eddies in the model except occasionally in the southern part of our region. In
649 the real world the modulation of mixing seen in Fig. 14 extends into the Northwest Arabian
650 Sea and the Gulf of Oman.

651

652 **5 Conclusions**

653 Our analysis of bloom variability in the northwestern Arabian Sea and Gulf of Oman has
654 illustrated both similar and dissimilar descriptive features between satellites and a suite of
655 models and explored the various mechanisms involved. Satellite analyses demonstrate the
656 existence of two blooms, the stronger one associated with the Southwest Monsoon and the
657 weaker one associated with the Northeast Monsoon as also shown by Madhupratap et al.
658 (1996), Kawamiya and Oschlies (2003), Murtugudde et al. (2007), and Al-Azri et al. (2010).
659 We demonstrate a pronounced anti-correlation between SSHA and chlorophyll blooms during
660 certain times in northern winter but a much weaker relationship in other months (typically
661 northern summer) with the relationship disappearing as the blooms vanish in the months of
662 April and May (northern spring). While the depth of thermocline and nutricline and also the
663 stratification affect the convection during the Northeast Monsoon (Dickey et al., 1998; Kumar
664 et al., 2001; Wiggert et al., 2002), we show that a thin nutricline/thermocline and a strong
665 stratification are also required to enable cold eddies to bring nutrients to euphotic zone and
666 develop phytoplankton blooms. During the wintertime monsoon, while both cooling in the
667 winter and eddies control the blooms, variability in bloom location will arise from variability
668 in the location of eddies, and so may not be predictable. In contrast, during the Southwest
669 Monsoon the dominant upwelling associated with the intense environmental forcing
670 supersedes the effect of eddies and the activity of the cold eddies is not pronounced.

671 Understanding of this phenomenon has been sought using five different 3D ocean-atmosphere
672 models, including a CORE-forced ocean with the TOPAZ biogeochemistry, a coupled model
673 with the TOPAZ biogeochemistry and CM2.6. Because the coarse models with TOPAZ are
674 not able to capture eddies and the interannual variability, CM2.6 (miniBLING), an eddy-
675 resolving high resolution model, was also considered for simulating the spatial and temporal
676 changes of the bloom in the region. This model simulates the two blooms seen in the data and
677 shows that the nutrients driving the northern summer bloom are supplied by advection while
678 those driving the wintertime bloom are supplied by vertical diffusion. However, this model is
679 unable to simulate the seasonal relationship observed in the satellite products between blooms
680 and sea surface height. Although there is some anti-correlation, it tends to be associated with
681 larger spatial scales and not really related to eddies. Instead, eddies in the model usually wrap
682 the chlorophyll around themselves, producing high chlorophyll concentrations around their
683 edges and not at their centers. Comparing the model results to field measurements (WOA09)

Anand 1/7/2016 11:09 AM

Deleted: a set of

Anand 1/7/2016 11:09 AM

Deleted: d among

Anand 1/7/2016 11:09 AM

Deleted: verified

Anand 1/7/2016 11:10 AM

Deleted: m

Anand 1/7/2016 11:10 AM

Deleted: M

Shahabeddin Torabian 1/6/2016 9:08 PM

Deleted: in

Anand 1/7/2016 11:10 AM

Deleted: are

Anand 1/7/2016 11:10 AM

Deleted: ing

Anand 1/7/2016 11:10 AM

Deleted: o

Shahabeddin Torab... 1/12/2016 8:23 PM

Deleted: three

694 showed that the model does not account for the strong thermocline and nutricline in the
695 northern part of the region. In the wintertime, this leads to excessive convective supply of
696 nutrients and too strong of a bloom. However, for a few cases, eddies with [blooms](#) at the
697 center are tracked in the southern part of the domain. In this region, consistency is observed
698 between the model results and the field data. Analysis of the term balances in mixed layer
699 show that eddies in this region modulate the diffusive supply of nutrients. We suggest that
700 what happens in the model in the Southern Arabian Sea actually describes the Arabian Sea as
701 a whole according to the observations and the field data. The model misses the eddy signal in
702 the north because it lacks a thin nutricline, motions of which will lead to differences in
703 nutrient supply. In the real world, eddies modulate the diffusive supply of nutrients during the
704 wintertime and there is more mixing in the eddy centers along with the diffusive supply
705 provided by the cooling in the wintertime.

706 Accordingly, there is a potential to improve the numerical models by better simulating the
707 Persian Gulf Outflow to produce a sharper thermocline, allowing more realistic nutrient
708 supply. [Overflows are difficult to simulate in level-coordinate](#) models because they are prone
709 to excessive entrainment of the dense plume (Winton et al., 1998). While significant effort
710 has gone into simulating the Denmark Straits overflow at coarse [resolution](#) (Legg et al.,
711 2009), [our results show that smaller overflows such as the Persian Gulf may be regionally](#)
712 [significant. This may provide further impetus for using isopycnal models in high resolution](#)
713 [simulations, as such models can potentially simulate such overflows with greater fidelity.](#)

714 It is worth noting that regional models, (such as Resplandy et al. (2011)) do have the potential
715 to better simulate the hydrography of the Northern Arabian Sea. Because such models are
716 very tightly constrained through “sponges” that restore hydrography at the boundaries, they
717 may not have the problems that global models do at representing the effects of overflows that
718 they do not properly simulate. However, such models cannot by themselves simulate the
719 effects of changing climate, which in turn changes the boundary conditions. For this reason,
720 global models must still be used for projection, making it important to identify the reasons
721 that they are not going to work.

722
723
724

Shahabeddin Torab..., 1/12/2016 8:11 PM
Deleted: a bloom

726 **Acknowledgements**

727 The authors thank Eric Galbraith, Shahabeddin Torabian, Grace Kim, Carlos del Castillo, and
728 Jeremy Wardell for useful discussions. We also thank Rick Slater and Whit Anderson for
729 their support of the model simulations. Argo climatology data were collected and made freely
730 available by the International Argo Program and the national programs that contribute to it.
731 (<http://www.argo.ucsd.edu>, <http://argo.jcommops.org>). The Argo Program is part of the
732 Global Ocean Observing System.

733

734

735 **References**

- 736 Adcroft, A., Campin, J.-M., Hill, C. and Marshall, J.: Implementation of an Atmosphere–
737 Ocean General Circulation Model on the Expanded Spherical Cube, *Mon. Weather Rev.*,
738 132(12), 2845–2863, doi:10.1175/MWR2823.1, 2004.
- 739 Al-Azri, A. R., Piontkovski, S. A., Al-Hashmi, K. A., Goes, J. I., Gomes, H. D. R. and
740 Glibert, P. M.: Mesoscale and Nutrient Conditions Associated with the Massive 2008
741 *Cochlodinium polykrikoides* Bloom in the Sea of Oman/Arabian Gulf, *Estuaries and Coasts*,
742 doi:10.1007/s12237-013-9693-1, 2013.
- 743 Al-Azri, A. R., Piontkovski, S. A., Al-Hashmi, K. A., Goes, J. I. and Gomes, H. R.:
744 Chlorophyll a as a measure of seasonal coupling between phytoplankton and the monsoon
745 periods in the Gulf of Oman, *Aquat. Ecol.*, 44(2), 449–461, doi:10.1007/s10452-009-9303-2,
746 2010.
- 747 Anderson, D. M. and Prell, W. L.: A 300 KYR Record of Upwelling Off Oman During the
748 Late Quaternary: Evidence of the Asian Southwest Monsoon, *Paleoceanography*, 8(2), 193–
749 208, 1993.
- 750 ARGO: Climatology, [online] Available from: <http://www.argo.ucsd.edu>, 2015.
- 751 Armstrong, R. A., Lee, C., Hedges, J. I., Honjo, S. and Wakeham, S. G.: A new, mechanistic
752 model for organic carbon fluxes in the ocean based on the quantitative association of POC
753 with ballast minerals, *Deep. Res. Part II Top. Stud. Oceanogr.*, 49(1-3), 219–236,
754 doi:10.1016/S0967-0645(01)00101-1, 2002.
- 755 Banse, K. and McClain, C. R.: Winter blooms of phytoplankton in the Arabian Sea as
756 observed by the Coastal Zone Color Scanner, *Mar Ecol Prog Ser*, 34, 201–211, 1986.
- 757 Barimalala, R., Bracco, A., Kucharski, F., McCreary, J. P. and Crise, A.: Arabian Sea
758 ecosystem responses to the South Tropical Atlantic teleconnection, *J. Mar. Syst.*, 117-118,
759 14–30, doi:10.1016/j.jmarsys.2013.03.002, 2013.
- 760 Bartolacci, D. M. and Luther, M. E.: Patterns of co-variability between physical and
761 biological parameters in the Arabian Sea, *Deep Sea Res. Part II Top. Stud. Oceanogr.*, 46(8-
762 9), 1933–1964, doi:10.1016/S0967-0645(99)00049-1, 1999.
- 763 Behrenfeld, M. J.: Abandoning Sverdrup’s Critical Depth Hypothesis on phytoplankton
764 blooms, *Ecology*, 91(4), 977–989, doi:10.1890/09-1207.1, 2010.
- 765 Behrenfeld, M. J., Boss, E., Siegel, D. A. and Shea, D. M.: Carbon-based ocean productivity
766 and phytoplankton physiology from space, *Global Biogeochem. Cycles*, 19(1), 1–14,
767 doi:10.1029/2004GB002299, 2005.
- 768 Bryan, K. and Lewis, L. J.: A Water Mass Moel of the World Ocean, 84(8), 2503, 1979.
- 769 Danabasoglu, G., Large, W. G., Tribbia, J. J., Gent, P. R., Briegleb, B. P. and McWilliams, J.
770 C.: Diurnal coupling in the tropical oceans of CCSM3, *J. Clim.*, 19(11), 2347–2365,
771 doi:10.1175/JCLI3739.1, 2006.
- 772 Delworth, T. L., Broccoli, A. J., Rosati, A., Stouffer, R. J., Balaji, V., Beesley, J. A., Cooke,
773 W. F., Dixon, K. W., Dunne, J., Dunne, K. A., Durachta, J. W., Findell, K. L., Ginoux, P.,
774 Gnanadesikan, A., Gordon, C. T., Griffies, S. M., Gudgel, R., Harrison, M. J., Held, I. M.,
775 Hemler, R. S., Horowitz, L. W., Klein, S. A., Knutson, T. R., Kushner, P. J., Langenhorst, A.
776 R., Lee, H. C., Lin, S. J., Lu, J., Malyshev, S. L., Milly, P. C. D., Ramaswamy, V., Russell, J.,

778 Schwarzkopf, M. D., Shevliakova, E., Sirutis, J. J., Spelman, M. J., Stern, W. F., Winton, M.,
779 Wittenberg, A. T., Wyman, B., Zeng, F. and Zhang, R.: GFDL's CM2 global coupled climate
780 models. Part I: Formulation and simulation characteristics, *J. Clim.*, 19(5), 643–674,
781 doi:10.1175/JCLI3629.1, 2006.

782 Delworth, T. L., Rosati, A., Anderson, W., Adcroft, A. J., Balaji, V., Benson, R., Dixon, K.,
783 Griffies, S. M., Lee, H.-C., Pacanowski, R. C., Vecchi, G. A., Wittenberg, A. T., Zeng, F. and
784 Zhang, R.: Simulated Climate and Climate Change in the GFDL CM2.5 High-Resolution
785 Coupled Climate Model, *J. Clim.*, 25(8), 2755–2781, doi:10.1175/JCLI-D-11-00316.1, 2012.

786 Dickey, T., Marra, J., Sigurdson, D. E., Weller, R. A., Kinkade, C. S., Zedler, S. E., Wiggert,
787 J. D. and Langdon, C.: Seasonal variability of bio-optical and physical properties in the
788 Arabian Sea : October 1994 — October 1995, *Deep. Res. II*, 45(October 1994), 2001–2025,
789 1998.

790 Dunne, J., Gnanadesikan, A., Sarmiento, J. L. and Slater, R. D.: Technical description of the
791 prototype version (v0) of Tracers Of Phytoplankton with Allometric Zooplankton (TOPAZ)
792 ocean biogeochemical model as used in the Princeton IFMIP* model, *Biogeosciences Suppl.*,
793 7(1), 3593, doi:10.5194/bg-7-3593-2010, 2010.

794 Dunne, J. P., John, J. G., Adcroft, A. J., Griffies, S. M. and Hallberg, R. W.: GFDL's ESM2
795 Global Coupled Climate-Carbon Earth System Models. Part I: Physical Formulation and
796 Baseline Simulation Characteristics, *J. Clim.*, 25, 6646–6665,
797 doi:http://dx.doi.org/10.1175/JCLI-D-11-00560.1, 2012.

798 Dunne, J. P., John, J. G., Shevliakova, S., Stouffer, R. J., Krasting, J. P., Malyshev, S. L.,
799 Milly, P. C. D., Sentman, L. T., Adcroft, A. J., Cooke, W., Dunne, K. A., Griffies, S. M.,
800 Hallberg, R. W., Harrison, M. J., Levy, H., Wittenberg, A. T., Phillips, P. J. and Zadeh, N.:
801 GFDL's ESM2 global coupled climate-carbon earth system models. Part II: Carbon system
802 formulation and baseline simulation characteristics, *J. Clim.*, 26(7), 2247–2267,
803 doi:10.1175/JCLI-D-12-00150.1, 2013.

804 Dunne, J. P., Sarmiento, J. L. and Gnanadesikan, A.: A synthesis of global particle export
805 from the surface ocean and cycling through the ocean interior and on the seafloor, *Global*
806 *Biogeochem. Cycles*, 21(4), 1–16, doi:10.1029/2006GB002907, 2007.

807 | Ezam, M., Bidokhti, A. A. and Javid, A. H.: Numerical simulations of spreading of the Persian
808 Gulf outflow into the Oman Sea, *Ocean Sci.*, 6(4), 887–900, doi:10.5194/os-6-887-2010,
809 2010.

810 Fischer, A. S., Weller, R. A., Rudnick, D. L., Eriksen, C. C., Lee, C. M., Brink, K. H., Fox, C.
811 A. and Leben, R. R.: Mesoscale eddies, coastal upwelling, and the upper-ocean heat budget in
812 the Arabian Sea, *Deep Sea Res. Part II Top. Stud. Oceanogr.*, 49(12), 2231–2264,
813 doi:10.1016/S0967-0645(02)00036-X, 2002.

814 Fox-Kemper, B., Ferrari, R. and Hallberg, R.: Parameterization of Mixed Layer Eddies. Part
815 I: Theory and Diagnosis, *J. Phys. Oceanogr.*, 38(6), 1145–1165, doi:10.1175/2007JPO3792.1,
816 2008.

817 Galbraith, E. D., Dunne, J. P., Gnanadesikan, A., Slater, R. D., Sarmiento, J. L., Dufour, C.
818 O., de Souza, G. F., Bianchi, D., Claret, M., Rodgers, K. B. and Sedigh Marvasti, S.:
819 Complex functionality with minimal computation: Promise and pitfalls of reduced-tracer
820 ocean biogeochemistry models, *J. Adv. Model. Earth Syst.*, 1–17,
821 doi:10.1002/2015MS000463, 2015.

- 822 Gaube, P., McGillicuddy, D., Chelton, D., Behrenfeld, M. J. and Strutton, P.: Regional
823 variations in the influence of mesoscale eddies on near-surface chlorophyll Peter, J. Geophys.
824 Res. Ocean., 119, 8195–8220, doi:10.1002/2014JC010111. Received, 2014.
- 825 Gnanadesikan, A., Dixon, K. W., Griffies, S. M., Balaji, V., Barreiro, M., Beesley, J. A.,
826 Cooke, W. F., Delworth, T. L., Gerdes, R., Harrison, M. J., Held, I. M., Hurlin, W. J., Lee, H.
827 C., Liang, Z., Nong, G., Pacanowski, R. C., Rosati, A., Russell, J., Samuels, B. L., Song, Q.,
828 Spelman, M. J., Stouffer, R. J., Sweeney, C. O., Vecchi, G., Winton, M., Wittenberg, A. T.,
829 Zeng, F., Zhang, R. and Dunne, J. P.: GFDL's CM2 global coupled climate models. Part II:
830 The baseline ocean simulation, *J. Clim.*, 19(5), 675–697, doi:10.1175/JCLI3630.1, 2006.
- 831 Gnanadesikan, A., Dunne, J. P. and John, J.: What ocean biogeochemical models can tell us
832 about bottom-up control of ecosystem variability, *ICES J. Mar. Sci.*, 68(6), 1030–1044,
833 doi:10.1093/icesjms/fsr068, 2011.
- 834 Gnanadesikan, A., Dunne, J. P. and Msadek, R.: Connecting Atlantic temperature variability
835 and biological cycling in two earth system models, *J. Mar. Syst.*, 133, 39–54,
836 doi:10.1016/j.jmarsys.2013.10.003, 2014.
- 837 Goes, J. I., Thoppil, P. G., Gomes, H. D. R. and Fasullo, J. T.: Warming of the Eurasian
838 landmass is making the Arabian Sea more productive., *Science*, 308(5721), 545–547,
839 doi:10.1126/science.1106610, 2005.
- 840 Gomes, R., Goes, J. I., Matondkar, S. G. P., Parab, S. G., Al-azri, A. R. N. and Thoppil, P. G.:
841 Deep-Sea Research I Blooms of *Noctiluca miliaris* in the Arabian Sea — An in situ and
842 satellite study, *Deep Sea Res. Part I Oceanogr. Res. Pap.*, 55, 751–765,
843 doi:10.1016/j.dsr.2008.03.003, 2008.
- 844 Griffies, S. M., Biastoch, A., Böning, C., Bryan, F., Danabasoglu, G., Chassignet, E. P.,
845 England, M. H., Gerdes, R., Haak, H., Hallberg, R. W., Hazeleger, W., Jungclaus, J., Large,
846 W. G., Madec, G., Pirani, A., Samuels, B. L., Scheinert, M., Gupta, A. Sen, Severijns, C. A.,
847 Simmons, H. L., Treguier, A. M., Winton, M., Yeager, S. and Yin, J.: Coordinated Ocean-ice
848 Reference Experiments (COREs), *Ocean Model.*, 26(1-2), 1–46,
849 doi:10.1016/j.ocemod.2008.08.007, 2009.
- 850 Griffies, S. M., Gnanadesikan, A., Dixon, K. W., Dunne, J. P., Gerdes, R., Harrison, M. J.,
851 Rosati, A., Russell, J. L., Samuels, B. L., Spelman, M. J., Winton, M. and Zhang, R.:
852 Formulation of an ocean model for global climate simulations, *Ocean Sci. Discuss.*, 2(3),
853 165–246, doi:10.5194/osd-2-165-2005, 2005.
- 854 Hamzehei, S. and Bidokhti, A.: Red tide monitoring in the Persian Gulf and Gulf of Oman
855 using MODIS sensor data., *Tech. J. ...*, 1100–1107, 2013.
- 856 Honjo, S., Dymond, J., Prell, W. and Ittekkot, V.: Monsoon-controlled export fluxes to the
857 interior of the Arabian Sea, *Deep. Res. II*, 46(1999), 1859–1902, 2000.
- 858 Kawamiya, M. and Oschlies, A.: An eddy-permitting , coupled ecosystem-circulation model
859 of the Arabian Sea : comparison with observations, *J. Mar. Syst.*, 38, 221–257, 2003.
- 860 Klaas, C. and Archer, D. E.: Association of sinking organic matter with various types of
861 mineral ballast in the deep sea: Implications for the rain ratio, *Global Biogeochem. Cycles*,
862 16(4), 1116, doi:10.1029/2001GB001765, 2002.
- 863 Kostadinov, T. S., Siegel, D. A. and Maritorena, S.: Retrieval of the particle size distribution
864 from satellite ocean color observations, *J. Geophys. Res.*, 114(C9), C09015,

865 doi:10.1029/2009JC005303, 2009.

866 Kumar, S. P., Ramaiah, N., Gauns, M., Sarma, V. V. S. S., Muraleedharan, P. M.,
867 Raghukumar, S., Kumar, M. D. and Madhupratap, M.: Physical forcing of biological
868 productivity in the Northern Arabian Sea during the Northeast Monsoon, *Deep. Res. II*, 48,
869 1115–1126, 2001.

870 Large, W. G., McWilliams, J. C. and Doney, S. C.: Oceanic vertical mixing: A review and a
871 model with a nonlocal boundary layer parameterization, *Rev. Geophys.*, 32(4), 363,
872 doi:10.1029/94RG01872, 1994.

873 Legg, S., Briegleb, B., Chang, Y., Chassignet, E. P., Danabasoglu, G., Ezer, T., Gordon, A.
874 L., Griffies, S., Hallberg, R., Jackson, L., Large, W., Özgükmen, T. M., Peters, H., Price, J.,
875 Riemenschneider, U., Wu, W., Xu, X. and Yang, J.: Improving oceanic overflow
876 representation in climate models: The Gravity Current Entrainment Climate Process Team,
877 *Bull. Am. Meteorol. Soc.*, 90(5), 657–670, doi:10.1175/2008BAMS2667.1, 2009.

878 Levy, M., Resplandy, L. and Lengaigne, M.: Oceanicmesoscale turbulence drives large
879 biogeochemical interannual variability atmiddle and high latitudes, *Geophys. Res. Lett.*,
880 41(7), 2467–2474, doi:10.1002/2014GL059608, 2014.

881 Levy, M., Shankar, D., Andre, J., Shenoi, S. S. C., Durand, F. and Montegut, C. D. B.: Basin-
882 wide seasonal evolution of the Indian Ocean ’ s phytoplankton blooms, *J. Geophys. Res.*,
883 112(C12014), 1–14, 2007.

884 Madhupratap, M., Kumar, S., Bhattathiri, P., Kumar, M., Raghukumar, S., Nair, K. and
885 Ramaiah, N.: Mechanism of the biological response to winter cooling in the northeastern
886 Arabian Sea, *Nature*, 384(12), 549–552, 1996.

887 Maritorena, S., Siegel, D. and Peterson, A. R.: Optimization of a semianalytical ocean color
888 model for global-scale applications., *Appl. Opt.*, 41(15), 2705–14, 2002.

889 McGillicuddy, D., Kosnyrev, V., Ryan, J. and Yoder, J.: Covariation of mesoscale ocean
890 color and sea-surface temperature patterns in the Sargasso Sea, *Deep. Res. II*, 48, 1823–1836,
891 2001.

892 Murtugudde, R., Seager, R. and Thoppil, P.: Arabian Sea response to monsoon variations,
893 *Paleoceanography*, 22(4), 1–17, doi:10.1029/2007PA001467, 2007.

894 Naqvi, S. W. A., Moffett, J. W., Gauns, M. U., Narvekar, P. V, Pratihary, A. K., Naik, H.,
895 Shenoy, D. M., Jayakumar, D. A., Goepfer, T. J., Patra, P. K., Al-Azri, A. and Ahmed, S. I.:
896 The Arabian Sea as a high-nutrient , low-chlorophyll region during the late Southwest
897 Monsoon, *Biogeosciences*, 7, 2091–2100, doi:10.5194/bg-7-2091-2010, 2010.

898 Piontkovski, S., Al-Azri, A. and Al-Hashmi, K.: Seasonal and interannual variability of
899 chlorophyll-a in the Gulf of Oman compared to the open Arabian Sea regions, *Int. J. Remote*
900 *Sens.*, 32(22), 7703–7715, doi:10.1080/01431161.2010.527393, 2011.

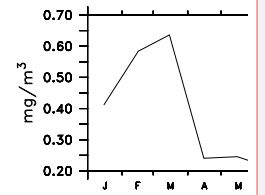
901 Piontkovski, S., Al-Gheilani, H., Jupp, B., Al-Azri, A. and Al-hashmi, K.: Interannual
902 Changes in the Sea of Oman Ecosystem., *Open Mar. Biol. J.*, 6, 38–52, 2012.

903 Resplandy, L., Lévy, M., Madec, G., Pous, S., Aumont, O. and Kumar, D.: Contribution of
904 mesoscale processes to nutrient budgets in the Arabian Sea, *J. Geophys. Res. Ocean.*, 116(11),
905 1–24, doi:10.1029/2011JC007006, 2011.

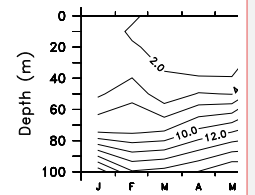
906 Richlen, M. L., Morton, S. L., Jamali, E. A., Rajan, A. and Anderson, D. M.: The catastrophic

- 907 2008–2009 red tide in the Arabian gulf region, with observations on the identification and
 908 phylogeny of the fish-killing dinoflagellate *Cochlodinium polykrikoides*, *Harmful Algae*,
 909 9(2), 163–172, doi:10.1016/j.hal.2009.08.013, 2010.
- 910 Sarma, Y. V. B., Al-hashmi, K. and Smith, L. S.: Sea Surface Warming and its Implications
 911 for Harmful Algal Blooms off Oman, *Int. J. Mar. Sci.*, 3(8), 65–71,
 912 doi:10.5376/ijms.2013.03.0008, 2013.
- 913 Shalapyonok, A., Olson, R. J. and Shalapyonok, L. S.: Arabian Sea phytoplankton during
 914 Southwest and Northeast Monsoons 1995 : composition , size structure and biomass from
 915 individual cell properties measured by flow cytometry, *Deep. Res. II*, 48, 1231–1261, 2001.
- 916 Simmons, H. L., Jayne, S. R., St. Laurent, L. C. and Weaver, A. J.: Tidally driven mixing in a
 917 numerical model of the ocean general circulation, *Ocean Model.*, 6(3-4), 245–263,
 918 doi:10.1016/S1463-5003(03)00011-8, 2004.
- 919 Stacey, M. W., Pond, S. and Nowak, Z. P.: A Numerical Model of the Circulation in Knight
 920 Inlet, British Columbia, Canada, *J. Phys. Oceanogr.*, 25(6), 1037–1062, doi:10.1175/1520-
 921 0485(1995)025<1037:ANMOTC>2.0.CO;2, 1995.
- 922 Tang, D., Kawamura, H. and Luis, A. J.: Short-term variability of phytoplankton blooms
 923 associated with a cold eddy in the northwestern Arabian Sea, *Remote Sens. Environ.*, 81, 82–
 924 89, 2002.
- 925 Veldhuis, M. J. W., Kraay, G. W., Van Bleijswijk, J. D. L. and Baars, M. A.: Seasonal and
 926 spatial variability in phytoplankton biomass , productivity and growth in the northwestern
 927 Indian Ocean : the southwest and northeast monsoon , 1992-1993, *Deep Sea Res. Part I*,
 928 44(3), 425–449, 1997.
- 929 Wang, D. and Zhao, H.: Estimation of phytoplankton responses to Hurricane Gonu over the
 930 Arabian Sea based on ocean color data, *Sensors*, 4878–4893, doi:10.3390/s8084878, 2008.
- 931 Wiggert, J. D., Murtugudde, R. G. and Christian, J. R.: Annual ecosystem variability in the
 932 tropical Indian Ocean : Results of a coupled bio-physical ocean general circulation model,
 933 *Deep. Res. II*, 53, 644–676, doi:10.1016/j.dsr2.2006.01.027, 2006.
- 934 Wiggert, J. D., Murtugudde, R. G. and McClain, C. R.: Processes controlling interannual
 935 variations in wintertime (Northeast Monsoon) primary productivity in the central Arabian
 936 Sea, *Deep. Res. II*, 49, 2319–2343, 2002.
- 937 Winton, M., Hallberg, R. and Gnanadesikan, A.: Simulation of Density-Driven Frictional
 938 Downslope Flow in Z -Coordinate Ocean Models, *J. Phys. Oceanogr.*, 28(11), 2163–2174,
 939 doi:10.1175/1520-0485(1998)028<2163:SODDFD>2.0.CO;2, 1998.
- 940

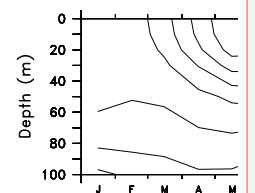
Shahabeddin Torab..., 1/12/2016 9:13 PM



(A) GSM Ch



(B) WOA09:

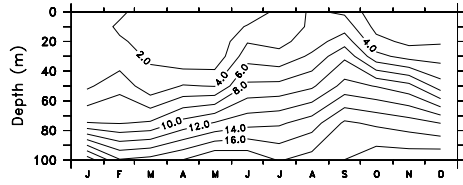


(C) WOA09: Water

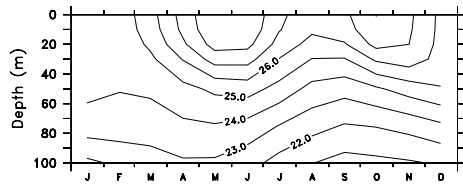
Deleted:



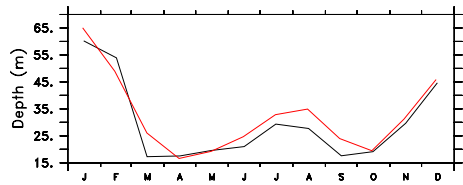
(A) GSM Chlorophyll a (mg/m^3)



(B) WOA09: Nitrate ($\mu\text{mol}/\text{l}$)

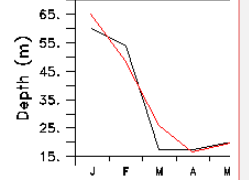


(C) WOA09: Water Temperature ($^{\circ}\text{C}$)



(D) MLD-WOA(Black) , MLD-Argo(Red)

Shahabeddin Torab... 1/12/2016 9:13 PM



(D) MLD-WOA

Deleted:

Unknown

Formatted: Font:12 pt

Unknown

Formatted: Font:(Default) Times New Roman, 12 pt, Font color: Red

942

943 Figure 1. Monthly average for region from 56°E-66°E, 15°N-26°N: (a) [Climatological surface](#)
 944 [chlorophyll-a \(SeaWIFS\) for a nominal year of 2001](#); (b) Nitrate (WOA09) over top 100m;
 945 (c) Temperature over top 100m; (d) WOA09 seasonal mixed layer depth in meters- [black line](#)
 946 [shows result from World Ocean Atlas, red line from ARGO climatology \(ARGO, 2015\).](#)

Anand 1/7/2016 11:20 AM

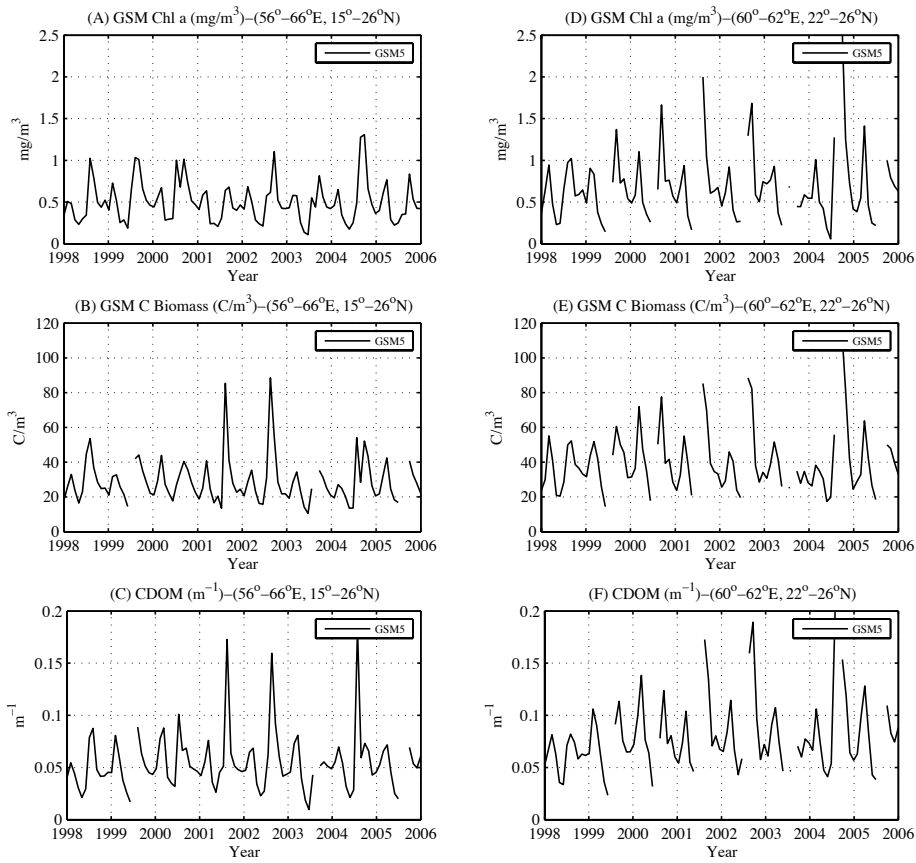
Deleted: s

Anand 1/7/2016 11:20 AM

Deleted: in 2001

Shahabeddin Torab... 1/10/2016 2:08 PM

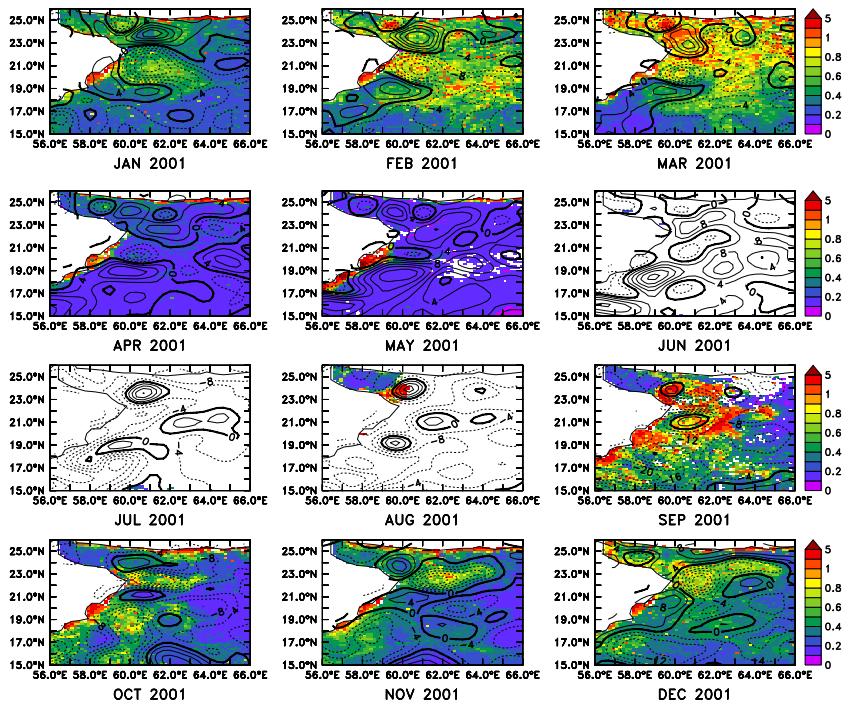
Formatted: Not Highlight



950

951 | Figure 2. Monthly variation of organic matter in [SeaWiFS](#) satellite data between 1998 and
 952 | 2005 within 56°-66°E, 15°-26°N (large region); and 60°-62°E, 22°-26°N (small region): (a)
 953 | and (d) chlorophyll; (b) and (e) particulate backscatter; (c) and (f) CDOM.

954

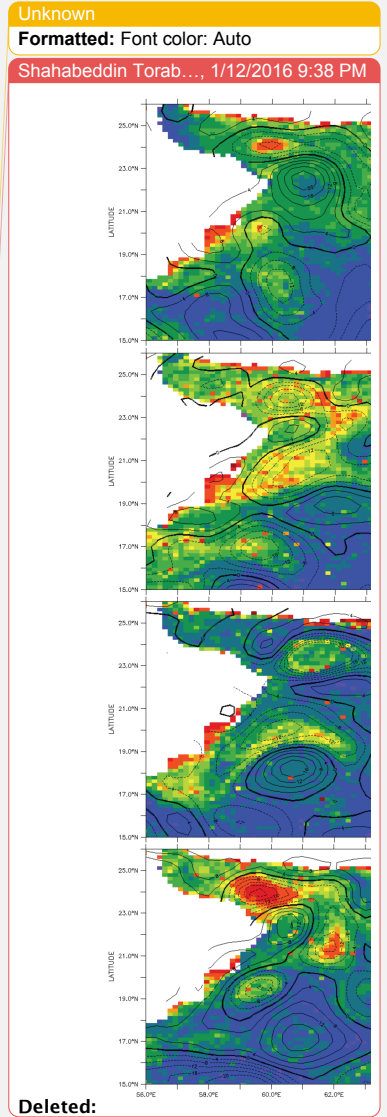
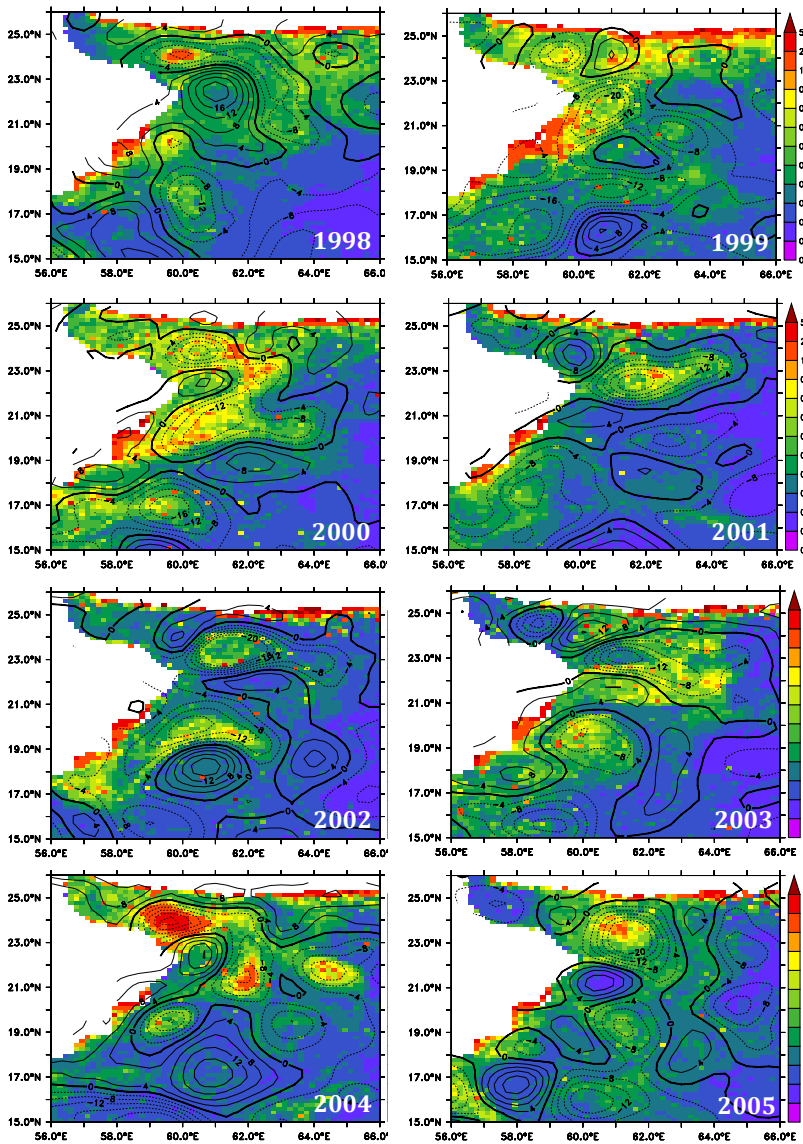


955

956 Figure 3. Satellite chlorophyll-a in mg/m^3 (colors) and sea-surface height anomaly (SSHA,
 957 contours) in cm (contour interval = 5cm) in the Gulf of Oman and Northwest Arabian Sea
 958 over the course of 2001.

959

- Anand 1/7/2016 11:22 AM
Deleted: C
- Anand 1/7/2016 11:22 AM
Deleted: S
- Anand 1/7/2016 11:22 AM
Deleted: S
- Anand 1/7/2016 11:24 AM
Deleted: meter



Deleted:

964

965 Figure 4. Chlorophyll-a in mgm^{-3} (colors) and sea surface height anomaly (SSHA, contours)
 966 in cm (contour interval=5 cm), in the Gulf of Oman and Northwest Arabian Sea during
 967 November in different years.

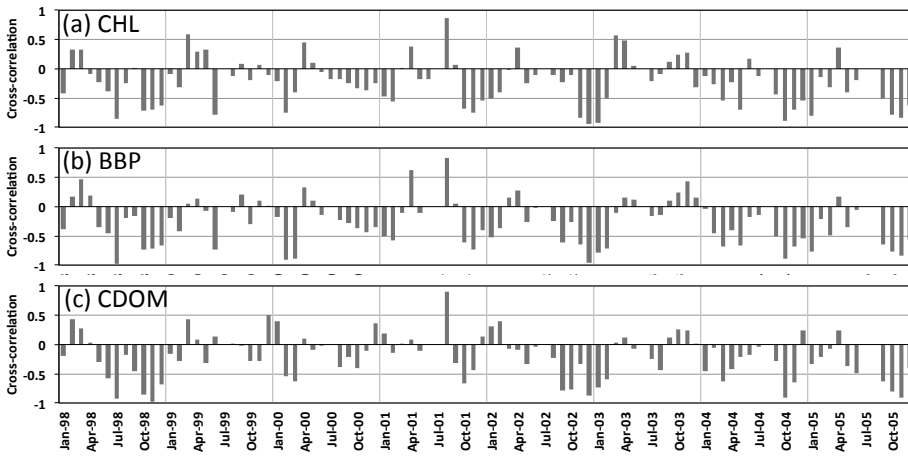
968

Anand 1/7/2016 11:25 AM

Deleted: meter

Anand 1/7/2016 11:23 AM

Deleted: in



972

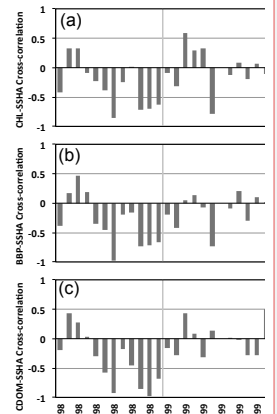
973 Figure 5. Monthly cross-correlation with AVISO SSHa between 1998 and 2005 within 56°-
 974 66°E and 15°-26°N. for (a) satellite-estimated chlorophyll; (b) satellite estimated BBP; (c)
 975 satellite-estimated CDOM.

976

Unknown

Formatted: Font color: Auto

Shahabeddin Torab..., 1/12/2016 8:50 PM



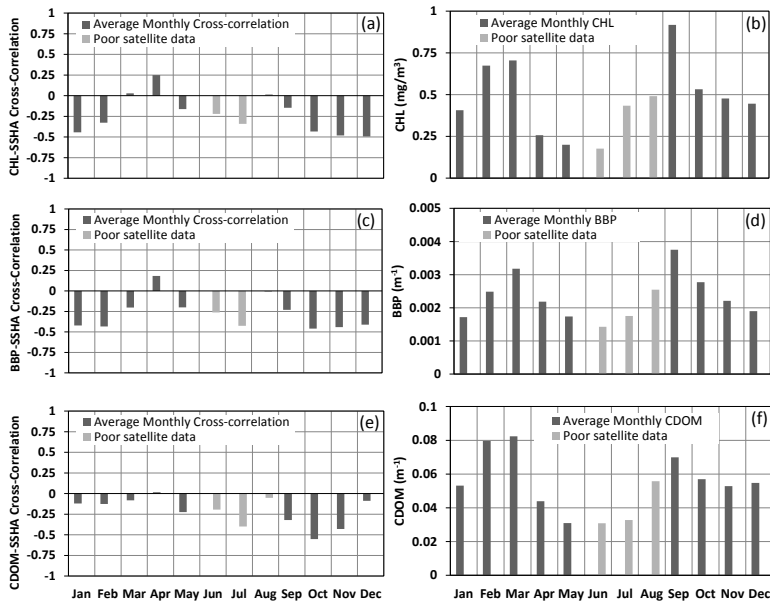
Deleted:

Anand 1/7/2016 11:26 AM

Deleted: y chlorophyll-SSHA

Anand 1/7/2016 11:25 AM

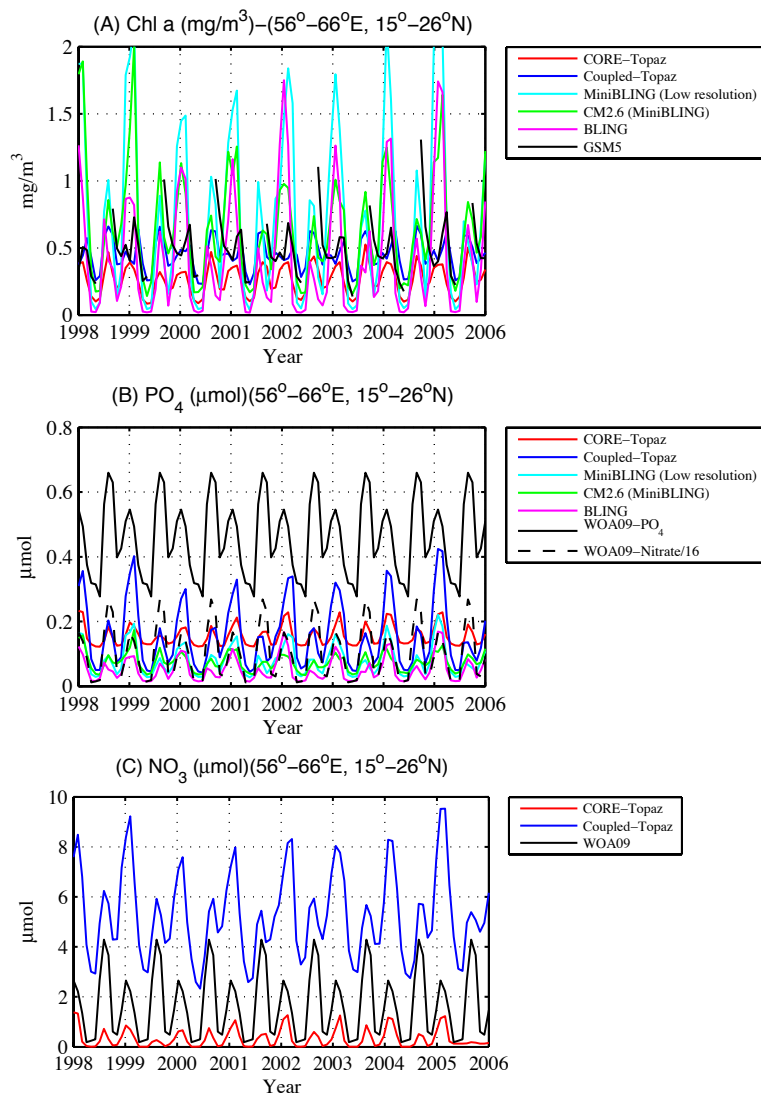
Deleted:



980

981 Figure 6. Average monthly cross-correlation with [observed](#) SSHA and average monthly
 982 values between 1998 and 2005 within 56°-66°E and 15°-26°N for (a, b) [satellite-estimated](#)
 983 chlorophyll; (c, d) [satellite-estimated](#) backscatter; (e, f) [satellite-estimated](#) CDOM.

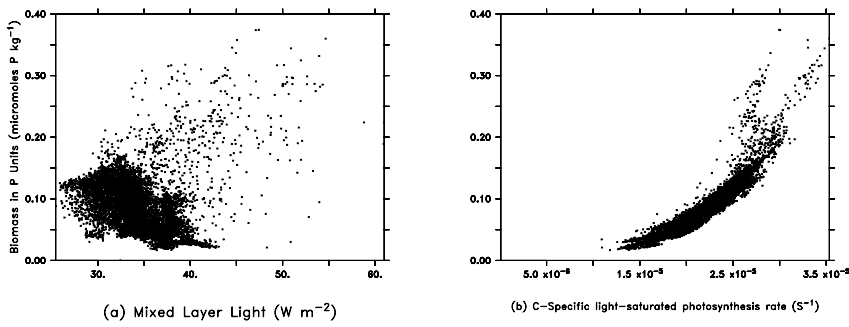
984



985

986 Figure 7. Monthly variation of organic matter in satellite data between 1998 and 2005 and
 987 GFDL models (8 characteristic years) within 56°–66°E, 15°–26°N: (a) chlorophyll from
 988 GFDL models and GSM5 algorithm. (b) PO₄ from the BLING and miniBLING simulations,
 989 NO₃/16 from the TOPAZ simulations and observed PO₄ from WOA09. (c) NO₃ from the
 990 TOPAZ simulations and observed NO₃ from WOA09.

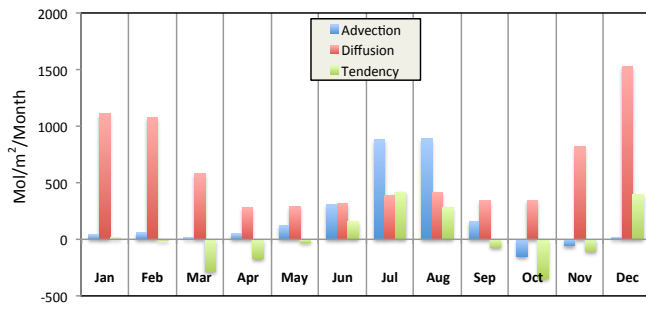
991



992
 993 Figure 8. Modeled biomass in CM2.6 in P units (mol P kg⁻¹) versus: (a) Mixed layer
 994 irradiance (Wm⁻²); (b) Light-Saturated photosynthesis rate (carbon specific) (s⁻¹) 56°-66°E,
 995 15°-26°N for January of year 195. In the model, biomass is a function of the growth rate
 996 smoothed over several days, and the light-saturated photosynthesis rate indicates the extent to
 997 which this growth rate is controlled by nutrient limitation.
 998

Unknown
 Formatted: Font color: Auto
 Shahabeddin Torab..., 1/12/2016 9:42 PM
 Deleted: Page Break

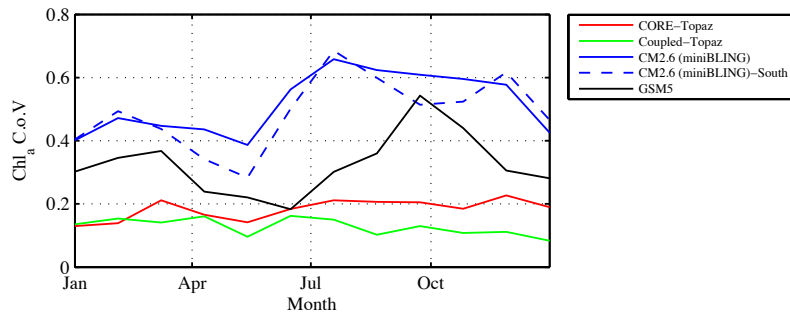
Unknown
 Formatted: Font color: Auto



1001

1002 Figure 9. PO₄ Advection, diffusion and tendency flux from the CM2.6 model over the whole
 1003 region averaged over top 50 m (56°-66°E, 15°-26°N).

1004



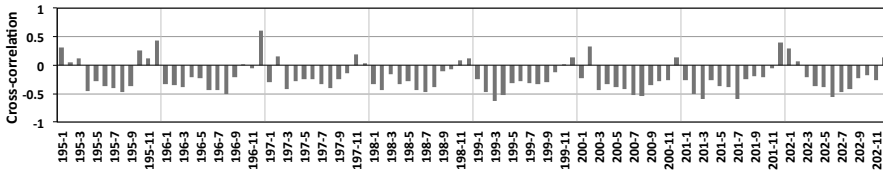
1006

1007 Figure 10. Average monthly coefficient of variation ([standard deviation/mean](#)) of Chlorophyll
 1008 a in satellite data between 1998 and 2005 and GFDL models (eight characteristics years)
 1009 within (56°–66°E, 15°–26°N) for the satellite data (black), CORE-TOPAZ (red), COUPLED-
 1010 TOPAZ (green) and CM2.6 model with miniBLING (blue) and within the south region (56°–
 1011 66°E, 15°–19°N) for CM2.6 (miniBLING, dashed blue).

1012

1013

1014



1015

Figure 11. CM2.6 monthly Chlorophyll-SSHA cross-correlation over 8 years within 56°-66°E

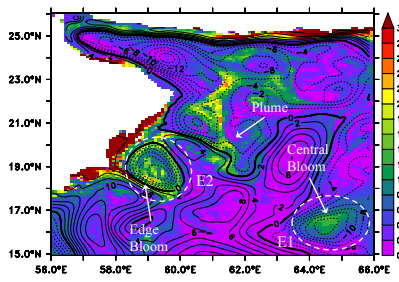
1016

and 15°-26°N.

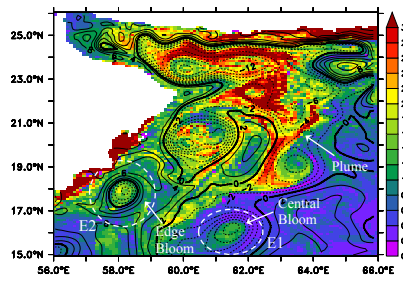
Unknown
Formatted: Font color: Auto
Shahabeddin Torab..., 1/12/2016 8:37 PM

Deleted:

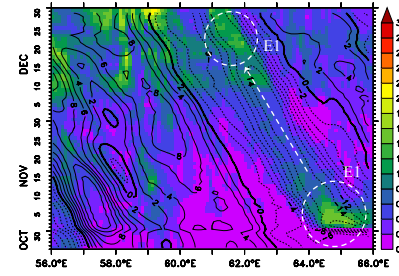
A smaller version of the bar chart from Figure 11, showing the same data for monthly Chlorophyll-SSHA cross-correlation from 195-1 to 202-11. The y-axis is labeled 'Chl-SSHA Cross-correlation' and ranges from -1 to 1. The x-axis shows years from 195-1 to 197-3. The bars fluctuate around zero, with a notable positive peak around 196-11 and a notable negative peak around 199-3.



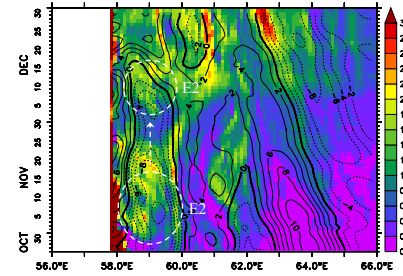
(a) Chlorophyll-a and SSHA at November 9th



(b) Chlorophyll-a and SSHA at December 28th



(c) Chlorophyll-a and SSHA: November and December along 16°N



(d) Chlorophyll-a and SSHA: November and December along 19°N

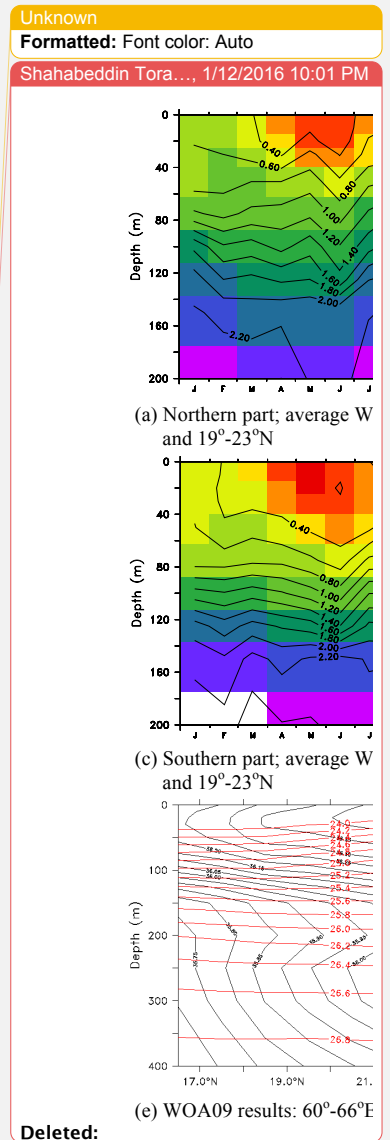
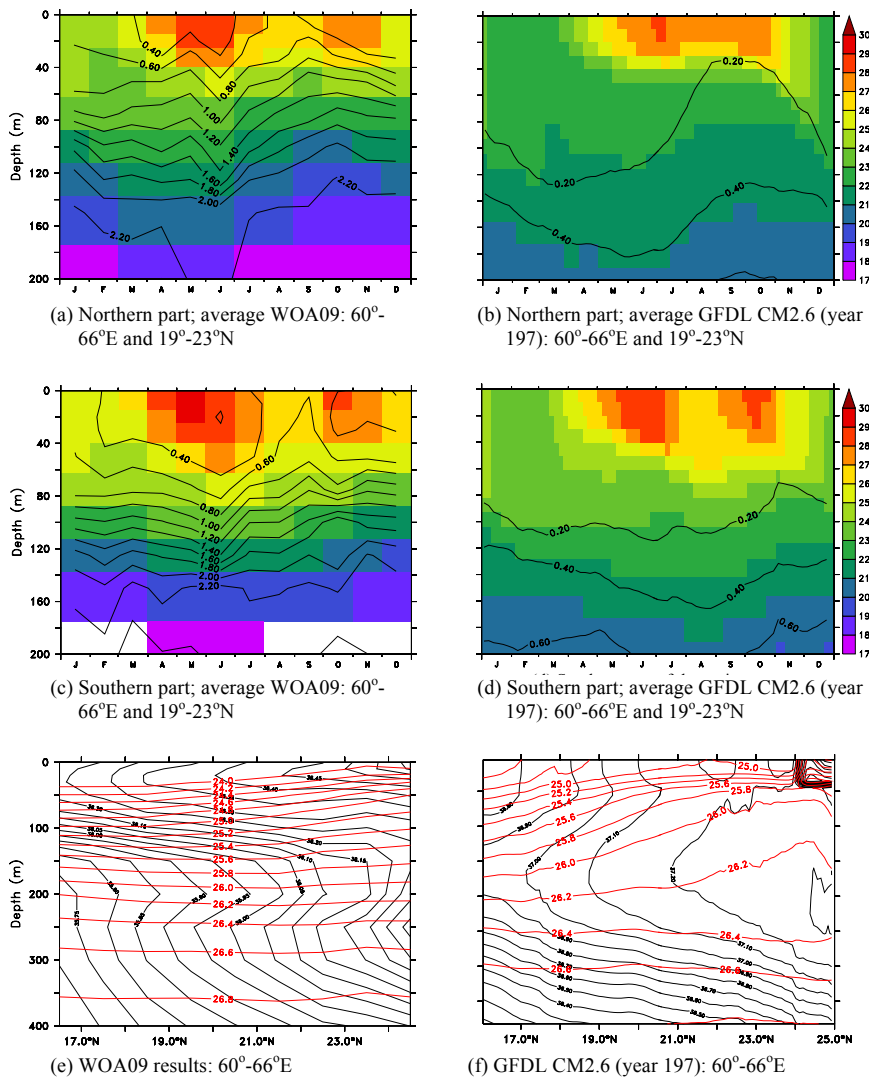
1018

1019 Figure 12. CM2.6 (miniBLING) Surface chlorophyll-a concentration and sea surface height
 1020 anomaly (SSHA) November and December during a year where the observed eddy-bloom
 1021 interaction is seen in the Southern part of the Arabian Sea.

1022

1023

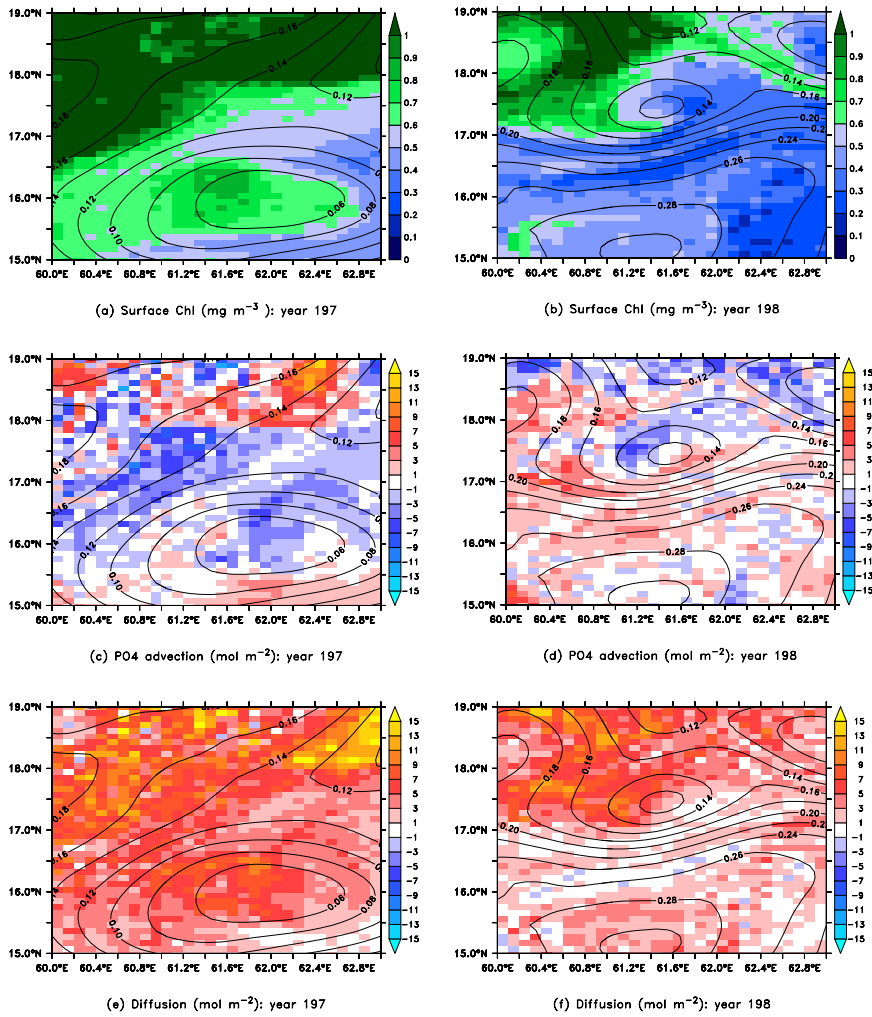
1024



1025

1026 Figure 13. (a-d) Seawater temperature (colors, °C) and Phosphate (PO₄) concentration
 1027 (contours, μM) for the northern (top row) and southern (middle row) parts of the central
 1028 Arabian Sea. ; (e-f) yearly averaged subsurface distribution of salinity (black contours) and
 1029 potential density (red contours). Left-hand column shows observations [with the Persian Gulf](#)
 1030 [plume centered at 300m](#), right-hand column results from CM2.6 model [with a much broader](#)
 1031 [mixing of salinity over the top 200m](#).

1032



1034

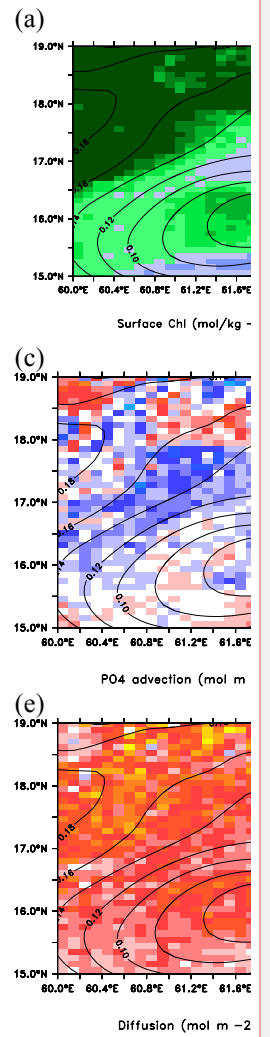
1035 Figure 14. Surface chlorophyll in mg/m^3 . (a-b), Advective flux of phosphate to top 50m
 1036 in mol/m^2 (c-d, colors), and diffusive flux of phosphate in mol/m^2 (e-f, colors) with sea surface
 1037 height (contours in m, contour interval 0.02m) for eddy E1 ($63^\circ\text{-}66^\circ\text{E}$, $15^\circ\text{-}18^\circ\text{N}$) for the
 1038 month of December during the two CM2.6 model years 197 and 198.

1039

Unknown

Formatted: Font color: Auto

Shahabeddin Torab..., 1/12/2016 9:49 PM

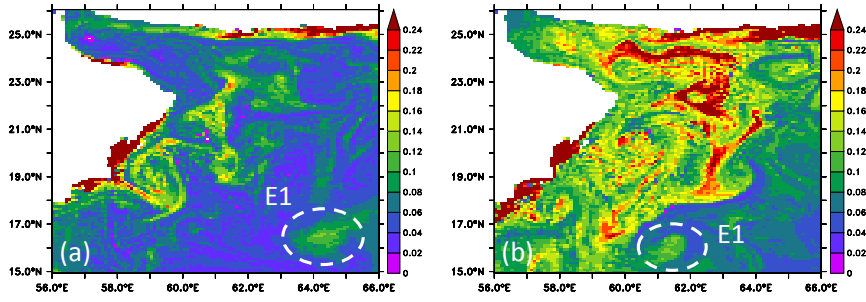


Deleted:

Anand 1/7/2016 11:36 AM

Deleted: overlaid

1042



1043

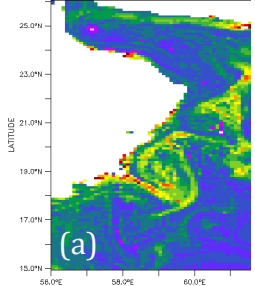
1044 Figure 15. (a), (b) : CM2.6 (miniBLING) PO_4 on 9 November and 28 December of year
1045 197.(56°–66° E, 15°–26° N).

1046

Unknown

Formatted: Font color: Auto

Shahabeddin Torab..., 1/12/2016 9:49 PM



Deleted:

Shahabeddin Torab..., 1/10/2016 9:56 AM

Deleted: P04

Shahabeddin Torab..., 1/10/2016 9:56 AM

Formatted: Subscript